

A Bayesian Numerical Homogenization Method for Elliptic Multiscale Inverse Problems*

Assyr Abdulle[†] and Andrea Di Blasio[†]

Abstract. A new strategy based on numerical homogenization and Bayesian techniques for solving multiscale inverse problems is introduced. We consider a class of elliptic problems which vary at a microscopic scale, and we aim at recovering the highly oscillatory tensor from measurements of the fine scale solution at the boundary, using a coarse model based on numerical homogenization and model order reduction. Assuming a known micro structure, our aim is to recover a macroscopic scalar parameterization of the microscale tensor. We provide a rigorous Bayesian formulation of the problem, taking into account different possibilities for the choice of the prior measure. We prove well-posedness of the effective posterior measure and, by means of G-convergence, we establish a link between the effective posterior and the fine scale model. Several numerical experiments illustrate the efficiency of the proposed scheme and confirm the theoretical findings.

Key words. inverse problems, Bayesian regularization, homogenization, multiscale methods

AMS subject classifications. 62G05, 65N21, 74Q05

DOI. 10.1137/18M1187891

1. Introduction. Inverse problems for partial differential equations (PDEs) play an important role in the sciences and engineering, with numerous applications such as geoscience or medical imaging, for example. In this work we are interested in PDEs characterized by the presence of variations on a very fine scale, which can be found, for example, in the study of composite materials or porous media. Let $\Omega \subset \mathbb{R}^d$, $d \geq 2$, be an open, bounded, connected set with sufficiently regular boundary $\partial\Omega$, and consider the problem of finding the weak solution $u^\varepsilon \in H^1(\Omega)$ such that

$$(1) \quad \begin{aligned} -\nabla \cdot (A^\varepsilon \nabla u^\varepsilon) &= 0 && \text{in } \Omega, \\ u^\varepsilon &= g && \text{on } \partial\Omega. \end{aligned}$$

The superscript in A^ε (respectively, u^ε) emphasizes that the tensor (the solution) varies on a fine scale proportional to ε , which is usually much smaller than the dimension of the domain Ω considered for application. The inverse problem we are interested in is to recover the highly oscillatory tensor A^ε based on observations originating from (1). Often standard numerical techniques such as the finite element method (FEM) are not appropriate to approximate (1) since mesh resolution at the finest scale is required to provide a reliable solution. Mesh resolution down to the ε scale can be prohibitively expensive when ε is small. This issue is even

*Received by the editors May 25, 2018; accepted for publication (in revised form) January 17, 2020; published electronically March 10, 2020.

<https://doi.org/10.1137/18M1187891>

Funding: This work is partially supported by the Swiss National Science Foundation, grant 200020_172710.

[†]École Polytechnique Fédérale de Lausanne, Lausanne, Switzerland (assyr.abdulle@epfl.ch, andrea.diblasio@epfl.ch).

more dramatic when solving inverse problems, since one typically needs multiple evaluations of (1), and thus an alternative approach is required. From the theory of homogenization [11, 13, 20] we know that there exists an effective tensor A^0 such that (up to a subsequence) the solution of (1) converges in a weak sense to the solution $u^0 \in H^1(\Omega)$ of the problem

$$(2) \quad \begin{aligned} -\nabla \cdot (A^0 \nabla u^0) &= 0 && \text{in } \Omega, \\ u^0 &= g && \text{on } \partial\Omega, \end{aligned}$$

where A^0 is referred to as the homogenized tensor. An explicit form of A^0 is usually not known, and so numerical homogenization [1, 2] is needed to obtain the homogenized solution u^0 based on data defining problem (1). Our strategy to efficiently retrieve the conductivity A^ε , based on observations originating from (1), relies on the reduced model (2). In [4] we analyzed and solved the inverse problem in the case where the observed quantities were defined by the Dirichlet to Neumann map associated to (1),

$$(3) \quad \Lambda_{A^\varepsilon} : g \in H^{1/2}(\partial\Omega) \mapsto A^\varepsilon \nabla u^\varepsilon \cdot \nu|_{\partial\Omega} \in H^{-1/2}(\partial\Omega),$$

where ν denotes the exterior unit normal to $\partial\Omega$.

In this paper, as in [4], we consider a class of parameterized multiscale locally periodic tensors of the form $A_{\sigma^*}^\varepsilon(x) = A(\sigma^*(x), x/\varepsilon)$, where $\sigma^* : \Omega \rightarrow \mathbb{R}$. We assume that the map $(t, x) \mapsto A(t, x/\varepsilon)$, $t \in \mathbb{R}$, $x \in \Omega$, is known while $\sigma^* : \Omega \rightarrow \mathbb{R}$ has to be determined to recover the whole tensor. A typical example of this setting could be represented by a multi-phase medium, whose constituent materials are known, but their respective volume fraction or macroscopic orientation are unknown. Or, we could think of an application in linear elasticity where the goal is to retrieve some elastic properties, e.g., the Young's modulus, of a high heterogeneous porous medium. This type of parameterized multiscale inverse problems was first introduced in [16], where it is shown that numerical homogenization can be used for solving parameterized multiscale inverse problems. Departing from [4], where in order to ensure well-posedness we solved the problem by means of Tikhonov regularization, we recast here the problem into a statistical framework and develop a multiscale numerical method based on Bayesian techniques. In addition, in contrast to [4], instead of considering observed data as living in some functional space, e.g., $H^{-1/2}(\partial\Omega)$, we consider discrete quantities in \mathbb{R} represented by the average of the normal flux at the boundary measured on different locations $\Gamma_j \subset \partial\Omega$, $j = 1, \dots, J$, $J \in \mathbb{N}$. For a survey on the Bayesian approach for inverse problems, we mention [12, 24]. For a rigorous Bayesian formulation of the inverse conductivity problem, known also as electrical impedance tomography, we also mention [14]. We mention that Bayesian multiscale inverse problems have also been addressed in [23]. The contribution of this paper can be summarized as follows:

- Due to the prohibitive cost of the forward problem in a multiscale context, we introduce an *effective forward problem* and a related *effective posterior measure*. The homogenization error introduced in this framework can be quantified in terms of G-convergence and we provide an offline algorithm to correct for the model discrepancy.
- Our numerical algorithm makes use of multiscale methods and model order reduction techniques to tackle computationally challenging multidimensional multiscale problems.

- Our methodology allows us to effectively recover a multiscale conductivity tensor through partial observations on the boundary of the domain.

Following [12, 24], we give a rigorous Bayesian formulation of the multiscale problem and prove the well-posedness of the effective posterior measure for our setting. We employ two different prior measures on the unknown coarse function and consider lognormal and level set priors. Moreover, we establish a link between the effective posterior measure and the fine scale model in terms of Hellinger distance, using G-convergence, to quantify the discrepancy between the homogenized data and the data originating from (1). The numerical method builds on the reduced basis finite element heterogeneous multiscale method (RB-FE-HMM) developed in [3]. Finally, inspired by [9], we approximate numerically the homogenization error distribution and we verify that including the homogenization error distribution in the definition of the posterior measure can significantly improve the results, especially when ε is relatively large.

The outline of the work is as follows. In section 2 we describe our setting for the observed data and we recall some useful tools for the Bayesian approach to inverse problems. In section 3 we state some preliminary results on well-posedness of the posterior measure and homogenization theory and we introduce two types of prior measures that will be used throughout the work. Our main results are presented in section 4. We prove existence and well-posedness of the effective posterior and establish the convergence of the Hellinger distance between the effective posterior and the posterior measure based on the full fine scale model. In section 5 we give a brief survey on the Markov chain Monte Carlo (MCMC) method used to sample from the posterior distribution, while in section 6 we explain how to approximate numerically (2) by a model order reduction multiscale method. Numerical experiments that illustrate our multiscale inverse method and confirm our theoretical findings are presented in section 7.

2. Preliminaries: Problem definition, homogenization, and G-convergence. Let Ω be an open and bounded set in \mathbb{R}^d . We consider a class of parameterized multiscale locally periodic tensors of the type $A_{\sigma^*}^\varepsilon(x) = A(\sigma^*(x), x/\varepsilon)$, where $\sigma^* : \Omega \rightarrow \mathbb{R}$. Given $g \in H^{1/2}(\partial\Omega)$, our aim is to recover $A_{\sigma^*}^\varepsilon$ from measurements originating from the model

$$\begin{aligned} -\nabla \cdot (A_{\sigma^*}^\varepsilon \cdot \nabla u^\varepsilon) &= 0 && \text{in } \Omega, \\ u^0 &= g && \text{on } \partial\Omega. \end{aligned}$$

Our unknown is represented by σ^* , while we assume to know the map $(t, y) \mapsto A(t, y)$, $t \in \mathbb{R}$, $y \in Y$, where $y = x/\varepsilon$, $y \in Y = (0, 1)^d$ and Y is the periodicity cell. In this work we will consider the family of parameterized tensors $(t, y) \mapsto A(t, y)$ such that, for any $0 < \sigma^- < \sigma^+ < \infty$, $t \mapsto A(t, y)$ is of class $C^1([\sigma^-, \sigma^+])$ and there exist $\alpha_{[\sigma^-, \sigma^+]}, \beta_{[\sigma^-, \sigma^+]} > 0$ such that

$$(4) \quad \alpha_{[\sigma^-, \sigma^+]} |b|^2 \leq A(t, y) b \cdot b, \quad |A(t, y)b| \leq \beta_{[\sigma^-, \sigma^+]} |b|, \quad \text{for a.e. } y \in Y \text{ and } \forall t \in [\sigma^-, \sigma^+], b \in \mathbb{R}^d.$$

Hence, we say that a macroscopic function $\sigma : \Omega \rightarrow \mathbb{R}$ will be admissible if there exist two constants σ^- and σ^+ , $0 < \sigma^- < \sigma^+ < \infty$, such that $\sigma^- \leq \sigma(x) \leq \sigma^+ \forall x \in \Omega$. Let us then introduce the admissible set which will be denoted by U and which is defined as

$$U = \{\sigma \in L^\infty(\Omega) : \sigma(x) > 0 \forall x \in \Omega\}.$$

We consider $J \in \mathbb{N}$ boundary portions of $\partial\Omega$, and we denote them as $\Gamma_j \subset \partial\Omega$, $j = 1, \dots, J$, $\Gamma_i \cap \Gamma_j = \emptyset$ for $i \neq j$. These portions of the boundary represent the locations at which the measurements are carried out. Moreover, the same experiment is reproduced for $L \in \mathbb{N}$ different Dirichlet data, which we denote as g_l , $l = 1, \dots, L$. Hence we have $J \times L$ observations. Then, we may introduce the forward operator $F^\varepsilon : U \rightarrow \mathbb{R}^{JL}$, $F^\varepsilon(\sigma) = \text{vec}(\{f_{jl}^\varepsilon(\sigma)\}_{\substack{1 \leq j \leq J \\ 1 \leq l \leq L}})$,

$$(5) \quad f_{jl}^\varepsilon(\sigma) = \langle \Lambda_{A_\sigma^\varepsilon} g_l, \phi_j \rangle_{H^{-1/2}(\partial\Omega), H^{1/2}(\partial\Omega)}, \quad j = 1, \dots, J, l = 1, \dots, L,$$

where $\Lambda_{A_\sigma^\varepsilon}$ is the Dirichlet to Neumann map (3) associated to the tensor $A_\sigma^\varepsilon(x) = A(\sigma(x), x/\varepsilon)$, and $\phi_j \in H^{1/2}(\partial\Omega)$ such that $\text{supp}(\phi_j) \subseteq \Gamma_j \forall j = 1, \dots, J$. In the following setting, we assume to dispose of a finite number of observations, corrupted by some noise, so that

$$(6) \quad z = F^\varepsilon(\sigma^*) + e, \quad e \sim \mathcal{N}(0, C_e),$$

where C_e is a given covariance matrix. Based on these measurements we would like to recover σ^* .

2.1. Likelihood. Let X be a Banach space and P some map $P : \theta \in X \mapsto \sigma \in U$. The introduction of X and P will be useful later on to build different prior measures on the admissible set U . Introducing this abstract framework is also useful to perform a rigorous analysis about the validity of our approach, which will be carried out in section 3. Let us define the potential function $\Phi^\varepsilon : X \times \mathbb{R}^{JL} \rightarrow \mathbb{R}$, which measures the distance between the observed data and the values produced by the observation model for some $\theta \in X$ as

$$(7) \quad \begin{aligned} \Phi^\varepsilon(\theta, z) &= \frac{1}{2} \|z - G^\varepsilon(\theta)\|_{C_e}^2 \\ &= \frac{1}{2} \langle z - G^\varepsilon(\theta), z - G^\varepsilon(\theta) \rangle_{C_e} \\ &= \frac{1}{2} (z - G^\varepsilon(\theta))^\top C_e^{-1} (z - G^\varepsilon(\theta)), \end{aligned}$$

where $G^\varepsilon = F^\varepsilon \circ P$. Simply trying to minimize (7) leads to an ill-posed problem. To ensure well-posedness we may add some regularization term (e.g., Tikhonov regularization) or recast the problem into a statistical framework, where all the quantities involved are treated as random variables (Bayesian approach). Differently from standard regularization techniques, which produce as a solution a single point estimate of the unknown, with the statistical approach the solution is represented by a probability measure, called the posterior probability measure. The posterior measure can then be used to infer about the parameter values and quantify their uncertainties.

2.2. Fine and coarse scale posteriors. In Bayesian theory, it is assumed that all the prior information we have about the unknown we are seeking for can be described by what is called the prior measure, which we denote here as μ_{pr} . Using (6) and applying Bayes' formula we obtain that the posterior measure of θ given z , denoted by $\mu^\varepsilon(\theta|z)$, is related to μ_{pr} through the Radon–Nikodym derivative

$$(8) \quad \frac{d\mu^\varepsilon(\theta|z)}{d\mu_{pr}(\theta)} \propto \exp(-\Phi^\varepsilon(\theta, z)).$$

Unfortunately trying to explore $\mu^\varepsilon(\theta|z)$ via sampling techniques such as MCMC methods is infeasible, due to the high computational effort needed to evaluate the model G^ε even for few realizations of $\theta \in X$. Hence, to drastically reduce the computational cost, we combine the inverse problem with a coarse graining strategy. To do so, let us recall briefly some results from homogenization theory [7, 13, 20], in particular the concept of G-convergence. We denote as $M(\alpha, \beta, \Omega)$ the space

$$M(\alpha, \beta, \Omega) = \left\{ A \in L^\infty(\Omega, Sym_d) : \alpha|b|^2 \leq A(x)b \cdot b, |A(x)b| \leq \beta|b| \forall b \in \mathbb{R}^d \text{ and a.e. in } \Omega \right\},$$

where Sym_d denotes the class of $d \times d$ symmetric real valued matrices.

Definition 1. Let $\{A^\varepsilon\}_{\varepsilon>0}$ be a sequence of matrices in $M(\alpha, \beta, \Omega)$. We say that $\{A^\varepsilon\}_{\varepsilon>0}$ G-converges to the matrix $A^0 \in M(\alpha, \beta, \Omega)$ if and only if for every function $f \in H^{-1}(\Omega)$, $g \in H^{1/2}(\partial\Omega)$, the solution u^ε of

$$(9) \quad \begin{aligned} -\nabla \cdot (A^\varepsilon \nabla u^\varepsilon) &= f && \text{in } \Omega, \\ u^\varepsilon &= g && \text{on } \partial\Omega \end{aligned}$$

is such that

$$u^\varepsilon \rightharpoonup u^0 \quad \text{weakly in } H^1(\Omega),$$

where u^0 is the unique solution of

$$(10) \quad \begin{aligned} -\nabla \cdot (A^0 \nabla u^0) &= f && \text{in } \Omega, \\ u^0 &= g && \text{on } \partial\Omega. \end{aligned}$$

A consequence of G-convergence is the weak convergence of the flux

$$A^\varepsilon \nabla u^\varepsilon \rightharpoonup A^0 \nabla u^0 \quad \text{weakly in } (L^2(\Omega))^d.$$

Theorem 1 (see [11, 20], for example). One has the following compactness result. Let $\{A^\varepsilon\}_{\varepsilon>0}$ be a sequence of matrices in $M(\alpha, \beta, \Omega)$. Then there exists a subsequence $\{A^{\varepsilon'}\}_{\varepsilon'>0}$ and a matrix $A^0 \in M(\alpha, \beta, \Omega)$ such that $\{A^{\varepsilon'}\}_{\varepsilon'>0}$ G-converges to A^0 .

In particular, we consider for a $\sigma \in U$ the sequence of Y -periodic matrices defined by

$$A_\sigma^\varepsilon(x) = \{A_{ij}^\varepsilon(x)\}_{1 \leq i,j \leq d} \quad \text{a.e. on } \mathbb{R}^d,$$

where

$$A_{ij}^\varepsilon(x) = A_{ij}(\sigma(x), x/\varepsilon) = A_{ij}(\sigma(x), y), \quad A_{ij}(\sigma(x), \cdot) \text{ is } Y\text{-periodic,}$$

$\forall x \in \Omega$, $\forall i, j = 1, \dots, d$, and Y denotes the reference unit cell $(0, 1)^d$. Such tensors are usually referred to as locally periodic in the literature. In this particular case we have that the whole sequence $\{A_\sigma^\varepsilon\}_{\varepsilon>0}$ G-converges to the tensor $A_\sigma^0 \in M(\alpha_{[\sigma^-, \sigma^+]}, \beta_{[\sigma^-, \sigma^+]}, \Omega)$, $A_\sigma^0(x) = A^0(\sigma(x)) = \{A_{ij}^0(\sigma(x))\}_{1 \leq i,j \leq d}$, which is elliptic and is given by

$$A_{ij}^0(\sigma(x)) = \int_Y A_{ij}(\sigma(x), y) dy - \sum_{k=1}^d \int_Y A_{ik}(\sigma(x), y) \frac{\partial \chi^j}{\partial y_k} dy \quad \forall i, j = 1, \dots, d.$$

The micro functions χ^j , $j = 1, \dots, d$, are defined to be the unique solutions of the cell problems: find $\chi^j(x, \cdot) \in W_{per}^1(Y)$ such that

$$\int_Y A(\sigma(x), y) \nabla_y \chi^j \cdot \nabla_y v dy = \int_Y A(\sigma(x), y) \mathbf{e}^j \cdot \nabla_y v dy \quad \forall v \in W_{per}^1(Y),$$

where $\{\mathbf{e}^j\}_{j=1}^d$ is the canonical basis of \mathbb{R}^d and

$$W_{per}^1(Y) = \left\{ v \in H_{per}^1(Y) : \int_Y v dy = 0 \right\},$$

and $H_{per}^1(Y)$ is defined as the closure of $C_{per}^\infty(Y)$ for the $H^1(Y)$ -norm (where $C_{per}^\infty(Y)$ denotes the subset of $C^\infty(\mathbb{R}^d)$ of periodic functions in Y).

Hence using homogenization theory, we may introduce the operator $F^0 : U \rightarrow \mathbb{R}^{JL}$, $F^0(\sigma) = \text{vec}(\{f_{jl}^0(\sigma)\}_{\substack{1 \leq j \leq J \\ 1 \leq l \leq L}}$,

$$(11) \quad f_{jl}^0(\sigma) = \langle \Lambda_{A_\sigma^0} g_l, \phi_j \rangle_{H^{-1/2}(\partial\Omega), H^{1/2}(\partial\Omega)}, \quad j = 1, \dots, J, l = 1, \dots, L,$$

where $\Lambda_{A_\sigma^0}$ is the Dirichlet to Neumann map associated to the tensor A_σ^0 , the homogenized tensor corresponding to A_σ^ε . Then, we can define a new potential function $\Phi^0 : X \times \mathbb{R}^{JL} \rightarrow \mathbb{R}$ as

$$(12) \quad \Phi^0(\theta, z) = \frac{1}{2} \|z - G^0(\theta)\|_{C_e}^2,$$

where $G^0 : F^0 \circ P$, and P is a map such that $P : X \rightarrow U$. As for the full fine scale model, we can invoke Bayes' formula to define a posterior measure $\mu^0(\theta|z)$ associated to the potential function (12) which satisfies

$$(13) \quad \frac{d\mu^0(\theta|z)}{d\mu_{pr}(\theta)} \propto \exp(-\Phi^0(\theta, z)).$$

We note that this new measure is much easier to explore via sampling techniques since the homogenized forward model $F^0 : U \rightarrow \mathbb{R}^{JL}$ can be approximated efficiently and independently of ε . However ignoring the fine scale fluctuations in the multiscale tensor A_σ^ε and using its homogenized counterpart A_σ^0 might introduce uncertainty in the parameter estimation, in particular for large values of ε far from the G-convergence limit. It will be shown in section 4.2 that this homogenization error (the difference between the maps G^ε and G^0) can be corrected for by assuming that it follows a Gaussian distribution. The validity of such a correction has been rigorously established in [22] for one-dimensional problems.

2.3. Prior measure. We consider the case where μ_{pr} is a Gaussian probability measure on the Banach space $X = C^0(\bar{\Omega})$, and we will show in section 4 that the assumptions of Theorem 2 are satisfied by μ_{pr} and Φ^0 given in (12), with $G^0 = F^0 \circ P$, where $P : \theta \in C^0(\bar{\Omega}) \mapsto \sigma \in U$ is some map such that if $\|\theta - \theta_n\|_{L^\infty(\Omega)} \rightarrow 0$, then $P(\theta_n) \rightarrow P(\theta)$ either uniformly or in

measure. In particular, we consider two different priors P_1 and P_2 , namely, lognormal and the level set priors. We emphasize that this is not the only possible choice but recall that for each selected prior measure an analysis of the continuity properties should be carried out in order to ensure stability of the posterior. We mention that the priors chosen in this work have several applications, e.g., lognormal random fields are a widely used choice in subsurface modeling, and hence are a natural starting point [19, 25]. We also mention that level set priors are widely used in reservoir simulations, e.g., to model channelized reservoir models [15, 26].

2.3.1. Lognormal prior. The first prior that we consider, denoted P_1 , is simply given by the exponential of a continuous function. Hence $P_1 : C^0(\bar{\Omega}) \mapsto \sigma \in U$ is defined by $P_1(\theta) = \exp(\theta)$. Using the continuity of P_1 we see that if $\theta \in C^0(\bar{\Omega})$ and $\{\theta_n\}_{n>0}$ is a sequence in $C^0(\bar{\Omega})$ such that $\|\theta - \theta_n\|_{L^\infty(\Omega)} \rightarrow 0$, then $\|P_1(\theta) - P_1(\theta_n)\|_{L^\infty(\Omega)} \rightarrow 0$. The prior measure μ_{pr} on θ will be a nondegenerate Gaussian measure $\mathcal{N}(\theta_{pr}, C_{pr})$ defined on a Banach space $C^0(\bar{\Omega})$.

We note that for the original unknown σ , we have $\sigma = \exp(\theta)$, $\theta \in C^0(\bar{\Omega})$ and

$$\exp(-\|\theta\|_{L^\infty(\Omega)}) \leq \sigma(x) \leq \exp(\|\theta\|_{L^\infty(\Omega)}) \quad \forall x \in \Omega.$$

For the ellipticity and continuity conditions (4) for the conductivity tensor, we can take $\sigma^- = \exp(-\|\theta\|_{L^\infty(\Omega)})$ and $\sigma^+ = \exp(\|\theta\|_{L^\infty(\Omega)})$. We observe that the quantities $\alpha_{[\sigma^-, \sigma^+]}$ and $\beta_{[\sigma^-, \sigma^+]}$ are monotonic nondecreasing functions of $\|\theta\|_{L^\infty(\Omega)}$, and we will use the notation

$$(14) \quad \alpha_{[\sigma^-, \sigma^+]} = \alpha_{\|\theta\|_{L^\infty(\Omega)}} , \quad \beta_{[\sigma^-, \sigma^+]} = \beta_{\|\theta\|_{L^\infty(\Omega)}} .$$

2.3.2. Level set prior. The second prior that we consider is a level set prior. The map $P_2 : C^0(\bar{\Omega}) \mapsto \sigma \in U$ is defined in the following way. Let $n \in \mathbb{N}$ and fix constants $-\infty = c_0 < \dots < c_n = \infty$. Given $\theta : \Omega \rightarrow \mathbb{R}$, we define $\Omega_i \subseteq \Omega$ as

$$\Omega_i = \{x \in \Omega : c_{i-1} \leq \theta(x) < c_i\} , \quad i = 1, \dots, n ,$$

so that $\bar{\Omega} = \cup_{i=1}^n \bar{\Omega}_i$ and $\Omega_i \cap \Omega_j = \emptyset$ for $i \neq j$. Let us also define the level sets

$$\Omega_i^0 = \bar{\Omega}_i \cap \bar{\Omega}_{i+1} = \{x \in \Omega : \theta(x) = c_i\} , \quad i = 1, \dots, n-1 .$$

Now given some strictly positive functions $f_1, \dots, f_n \in C^0(\bar{\Omega})$, we define the map $P_2 : C^0(\bar{\Omega}) \rightarrow U$ as

$$P_2(\theta) = \sum_{i=1}^n f_i \mathbb{1}_{\Omega_i} .$$

In particular we will consider f_i which are constant on Ω . For the continuity of the map P_2 , we have the following proposition given in [18] (we denote by $|\Omega_j|$ the measure of Ω_j).

Proposition 1 (see [18]). *Let $\{\theta_n\}_{n>0} \subset C^0(\bar{\Omega})$ converge to some $\theta \in C^0(\bar{\Omega})$ uniformly. Then $\{P_2(\theta_n)\}_{n>0}$ converges to $P_2(\theta)$ in $L^q(\Omega)$, $1 \leq q < \infty$, if and only if $|\Omega_i^0| = 0 \forall i = 1, \dots, n-1$. Let μ_{pr} be a Gaussian probability measure on $C^0(\bar{\Omega})$ and let $\theta \sim \mu_{pr}$. Then $|\Omega_i^0| = 0$ μ_{pr} -almost surely for $i = 1, \dots, n-1$.*

Our prior measure on $C^0(\bar{\Omega})$ will be as in the lognormal case a Gaussian measure $\mathcal{N}(\theta_{pr}, C_{pr})$. Going back to the original unknown, we note that each $\sigma = P_2(\theta)$ will be uniformly bounded below

For the ellipticity and continuity conditions (4) for the conductivity tensor, the quantities $\alpha_{[\sigma^-, \sigma^+]}$ and $\beta_{[\sigma^-, \sigma^+]}$ are also uniformly bounded with respect to θ .

2.3.3. Comments on prior modeling. There is an important issue which needs to be addressed regarding the prior modeling. Although we have separated the fine and coarse scales in the homogenized problem, any prior function on the coarse scale which charges a range of scales may excite the same length scales as those within the micro structure. The extent to which this happens is related to the rate of decay of the prior variance, as a function of scale, and can be controlled to minimize this issue. While this does not make an explicit clear break between coarse and fine, it enables a practical separation. Our numerical results reported in section 7 demonstrate that this is sufficient for a practical procedure.

3. Well-posedness of the posterior measure. In this section we recall some theoretical results about existence and well-posedness of the posterior measure. It is important to underline that existence and well-posedness of the posterior measure is typically determined from continuity properties of the forward operator entering in the definition of the potential function. Then, it is necessary to build prior measures such that every proposal lies in the function space on which the continuity properties of the forward operator are satisfied. Hence, some analysis on regularity properties of the forward operator is needed. This is carried on in what follows. We assume we have a prior Gaussian measure $\mu_{pr} = \mathcal{N}(\theta_{pr}, C_{pr})$ defined on a Banach space X , such that $\mu_{pr}(X) = 1$. Let $\mu^0(\theta|z)$ be a posterior measure that we assume as in section 2 to satisfy

$$(15) \quad \frac{d\mu^0(\theta|z)}{d\mu_{pr}(\theta)} = \frac{1}{K^0(z)} \exp(-\Phi^0(\theta, z)),$$

where $\Phi^0(\theta, z)$ is the potential defined in (12) and $K^0(z)$ is the normalization constant

$$K^0(z) = \int_X \exp(-\Phi^0(\theta, z)) \mu_{pr}(d\theta),$$

so that $\mu^0(\theta|z)$ is actually a probability measure.

Definition 2. Let μ^1 and μ^2 be two probability measures on a Banach space X . Assume that μ^1 and μ^2 are both absolutely continuous with respect to a common reference measure μ , defined on the same measure space. Then the Hellinger distance between μ^1 and μ^2 is defined as

$$d_{Hell}^2(\mu^1, \mu^2) = \frac{1}{2} \int_X \left(\sqrt{\frac{d\mu^1}{d\mu}} - \sqrt{\frac{d\mu^2}{d\mu}} \right)^2 d\mu.$$

The next theorem gives sufficient conditions on $\Phi^0 : X \times \mathbb{R}^{JL} \rightarrow \mathbb{R}$ and μ_{pr} for the posterior measure defined in (15) to be well-defined. For more details and a complete overview on the Bayesian approach to inverse problems we refer to [24] and [12].

Theorem 2 (see [24], [12], for example). Assume that μ_{pr} is a Gaussian measure on the Banach space X and that $\mu_{pr}(X) = 1$. In addition, assume that the function $\Phi^0 : X \times \mathbb{R}^{JL} \rightarrow \mathbb{R}$ and the measure μ_{pr} satisfy the following properties:

1. For every $r > 0$ there is a $K = K(r)$ such that $\forall \theta \in X$ and $\forall z \in \mathbb{R}^{JL}$ such that $\max\{\|\theta\|_X, \|z\|_{C_e}\} < r$

$$0 \leq \Phi^0(\theta, z) \leq K.$$

2. For any fixed $z \in \mathbb{R}^{JL}$ the function $\Phi^0(\cdot, z) : X \rightarrow \mathbb{R}$ is continuous μ_{pr} -almost surely.
3. For $z_1, z_2 \in \mathbb{R}^{JL}$ with $\max\{\|z_1\|_{C_e}, \|z_2\|_{C_e}\} < r$ and for every $\theta \in X$, there exists a function $M = M(r, \|\theta\|_X)$, $M : \mathbb{R}^+ \times \mathbb{R}^+ \rightarrow \mathbb{R}^+$, monotonic nondecreasing, such that

$$|\Phi^0(\theta, z_1) - \Phi^0(\theta, z_2)| \leq M(r, \|\theta\|_X) \|z_1 - z_2\|_{C_e}.$$

Then the posterior measure μ^0 given by (15) is a well-defined probability measure.

4. Moreover, if

$$M(r, \|\cdot\|_X) \in L^2_{\mu_{pr}}(X),$$

then μ^0 is Lipschitz in the data z , with respect to the Hellinger distance, i.e., if $\mu^0(\theta|z_1)$ and $\mu^0(\theta|z_2)$ are two measures corresponding to data z_1 and z_2 , then there is a constant $C = C(r) > 0$ such that, $\forall z_1, z_2$ with $\max\{\|z_1\|_{C_e}, \|z_2\|_{C_e}\} < r$,

$$d_{Hell}(\mu^0(\theta|z_1), \mu^0(\theta|z_2)) \leq C \|z_1 - z_2\|_{C_e}.$$

4. Main results. Here we discuss our main contributions. First, we recall part of a regularity result for the class of $d \times d$ symmetric matrix functions $t \rightarrow A^0(t)$ which was obtained in [4] based on continuity assumptions on the class of $d \times d$ (fine scale) symmetric matrix functions $(t, y) \rightarrow A(t, y)$, $y = x/\varepsilon$.

Lemma 1 (see Theorem 2.8 in [4]). Let $x/\varepsilon = y$, $y \in Y = (0, 1)^d$. Consider the class of $d \times d$ symmetric matrix functions $(t, y) \mapsto A(t, y)$, where $A_{ij}(t, \cdot)$ is Y -periodic, $\forall i, j = 1, \dots, d$, $t \in [\sigma^-, \sigma^+]$, $0 < \sigma^- < \sigma^+ < \infty$. Assume that the map $t \mapsto A(t, y)$ is of class $C^1([\sigma^-, \sigma^+])$ and that there exist $\alpha_{[\sigma^-, \sigma^+]}$ and $\beta_{[\sigma^-, \sigma^+]} > 0$ such that (4) holds. Then the homogenized map $t \mapsto A^0(t)$ satisfies

$$(16) \quad \alpha_{[\sigma^-, \sigma^+]} |b|^2 \leq A^0(t)b \cdot b, \quad |A^0(t)b| \leq \beta_{[\sigma^-, \sigma^+]} |b| \quad \forall t \in [\sigma^-, \sigma^+], b \in \mathbb{R}^d,$$

and there exists a constant $E_{[\sigma^-, \sigma^+]} > 0$ such that

$$(17) \quad |\partial_t A^0(t)| \leq E_{[\sigma^-, \sigma^+]} \quad \forall t \in [\sigma^-, \sigma^+].$$

Our goal is then to study the continuity of the forward operator $G^0 : C^0(\overline{\Omega}) \rightarrow \mathbb{R}^{JL}$ and analyze the homogenization error to establish a convergence result when switching from the fine scale to the homogenized forward model.

4.1. Continuity of the forward operator. The following lemma is the key result to establish the continuity of the effective forward operator.

Lemma 2. *Let the assumptions of Lemma 1 be satisfied. Let $\sigma \in U$ and the sequence $\{\sigma_n\}_{n>0}$ in U be such that*

1. $\{\sigma_n\}_{n>0}$ converges to σ uniformly,

or

2. $\{\sigma_n\}_{n>0}$ converges to σ in the Lebesgue measure and there exist σ^- and σ^+ , with $0 < \sigma^- < \sigma^+ < \infty$, such that $\sigma^- \leq \sigma_n(x) \leq \sigma^+ \forall x \in \bar{\Omega}$ and $\forall n > 0$.

Then the sequence $\{\Lambda_{A_\sigma^0} g\}_{n>0}$ converges to $\Lambda_{A_\sigma^0} g$ in $H^{-1/2}(\partial\Omega)$.

Proof. The first part of the result has been proved in [4]. For convenience we briefly recall the arguments. Let us define $w = A_\sigma^0 \nabla u^0(\sigma) - A_{\sigma_n}^0 \nabla u^0(\sigma_n)$. Observing that $w \in H(\Omega, \text{div})$ and using the continuity of the map $w \in H(\Omega, \text{div}) \mapsto w \cdot \boldsymbol{\nu} \in H^{-1/2}(\partial\Omega)$ we know that

$$\|w \cdot \boldsymbol{\nu}\|_{H^{-1/2}(\partial\Omega)} \leq \|w\|_{L^2(\Omega)}.$$

Note that if $\{\sigma_n\}_{n>0}$ converges to $\sigma \in U$ uniformly, then there exist σ^- and σ^+ such that for every n sufficiently large $\sigma^- \leq \sigma_n(x) \leq \sigma^+ \forall x \in \Omega$, and so $\alpha_{[\sigma^-, \sigma^+]}$, $\beta_{[\sigma^-, \sigma^+]}$, $E_{[\sigma^-, \sigma^+]}$ are uniformly bounded with respect to n . The same is true for sequences converging in the Lebesgue measure using the uniform boundedness assumption. Hence in what follows we will just refer to such quantities as α , β , E . Using the Cauchy–Schwarz inequality, (16), and (17) we obtain

$$\begin{aligned} \int_{\Omega} |w|^2 dx &= \int_{\Omega} A_{\sigma_n}^0 (\nabla u^0(\sigma) - \nabla u^0(\sigma_n)) \cdot w dx \\ &\quad + \int_{\Omega} (A_\sigma^0 - A_{\sigma_n}^0) \nabla u^0(\sigma) \cdot w dx \\ &\leq \beta \|\nabla u^0(\sigma) - \nabla u^0(\sigma_n)\|_{L^2(\Omega)} \|w\|_{L^2(\Omega)} \\ &\quad + E \left(\int_{\Omega} |\sigma - \sigma_n|^2 |\nabla u^0(\sigma)|^2 dx \right)^{1/2} \|w\|_{L^2(\Omega)}. \end{aligned} \tag{18}$$

It follows from the weak formulation of $u^0(\sigma)$ and $u^0(\sigma_n)$ that, $\forall v \in H_0^1(\Omega)$, we have that

$$\int_{\Omega} (A_\sigma^0 \nabla u^0(\sigma) - A_{\sigma_n}^0 \nabla u^0(\sigma_n)) \cdot \nabla v dx = 0.$$

Then

$$\int_{\Omega} A_\sigma^0 (\nabla u^0(\sigma) - \nabla u^0(\sigma_n)) \cdot \nabla v dx = \int_{\Omega} (A_{\sigma_n}^0 - A_\sigma^0) \nabla u^0(\sigma_n) \cdot \nabla v dx \quad \forall v \in H_0^1(\Omega).$$

By choosing $v = u^0(\sigma) - u^0(\sigma_n) \in H_0^1(\Omega)$, using the Cauchy–Schwarz inequality, (17), and (16), we obtain

$$\|\nabla u^0(\sigma) - \nabla u^0(\sigma_n)\|_{L^2(\Omega)} \leq \alpha^{-1} E \left(\int_{\Omega} |\sigma - \sigma_n|^2 |\nabla u^0(\sigma_n)|^2 dx \right)^{1/2}. \tag{19}$$

Inserting (19) into (18) we obtain

$$(20) \quad \|w\|_{L^2(\Omega)} \leq E(1 + \alpha^{-1}\beta) \left(\int_{\Omega} |\sigma - \sigma_n|^2 |\nabla u^0(\sigma)|^2 dx \right)^{1/2},$$

and by using Holder's inequality and Lax–Milgram we finally obtain

$$(21) \quad \begin{aligned} \|w\|_{L^2(\Omega)} &\leq E(1 + \alpha^{-1}\beta) \|\sigma - \sigma_n\|_{L^\infty(\Omega)} \|\nabla u^0(\sigma)\|_{L^2(\Omega)} \\ &\leq E\alpha^{-1}\beta(1 + \alpha^{-1}\beta) \|g\|_{H^{1/2}(\partial\Omega)} \|\sigma - \sigma_n\|_{L^\infty(\Omega)}. \end{aligned}$$

Now, if $\|\sigma - \sigma_n\|_{L^\infty(\Omega)} \rightarrow 0$ the result follows from (21). On the other hand if $|\sigma - \sigma_n| \rightarrow 0$ in measure, since $|\Omega| < \infty$ and $\nabla u^0(\sigma) \in (L^2(\Omega))^d$, we have also that the integrand of (20) $|\sigma - \sigma_n|^2 |\nabla u^0(\sigma)|^2 \rightarrow 0$ in measure (see Corollary 2.2.6 in [8], for example). Now, since $|\sigma - \sigma_n|$ is uniformly bounded by assumptions, the whole integrand is bounded by a scalar multiple of $|\nabla u^0(\sigma)|^2$. Therefore by applying the Lebesgue's dominated convergence theorem, we obtain that $|\sigma - \sigma_n|^2 |\nabla u^0(\sigma)|^2 \rightarrow 0$ in $L^1(\Omega)$, and the result follows. ■

Remark 1. The Lebesgue's dominated convergence theorem is stated for sequences converging almost everywhere. However, convergence almost everywhere can be replaced in this case by convergence in measure, since $|\Omega| < \infty$.

Remark 2. The result given in Lemma 2 is stronger than the one we obtained in Lemma 3.1 in [4], since it states continuity of the flux with respect to the convergence in measure of $\{\sigma_n\}_{n>0}$ to σ . In [4] the continuity of the flux with respect to the $L^r(\Omega)$ topology, with $1 \leq r < \infty$, was obtained by asking for higher regularity of the solution u^0 .

We can deduce the following lemma that establishes the continuity of the effective forward operator.

Lemma 3. *Let the assumptions of Lemma 2 be satisfied. Then the sequence $\{F^0(\sigma_n)\}_{n>0}$ converges to $F^0(\sigma)$.*

Proof. We have that

$$\begin{aligned} \|F^0(\sigma) - F^0(\sigma_n)\|_{C_e} &\leq C \sum_{j=1}^J \sum_{l=1}^L \left| \langle (\Lambda_{A_\sigma^0} - \Lambda_{A_{\sigma_n}^0}) g_l, \phi_j \rangle_{H^{-1/2}(\partial\Omega), H^{1/2}(\partial\Omega)} \right| \\ &\leq C \sup_l \|(\Lambda_{A_\sigma^0} - \Lambda_{A_{\sigma_n}^0}) g_l\|_{H^{-1/2}(\partial\Omega)} \sup_j \|\phi_j\|_{H^{1/2}(\partial\Omega)}, \end{aligned}$$

and the result follows from Lemma 2. ■

Finally, we establish that the posterior measure (13) based on the potential function Φ^0 is well-defined and Lipschitz continuous in the data with respect to the Hellinger distance.

Theorem 3. *Let the assumptions of Lemma 1 be satisfied. Let μ_{pr} be a Gaussian probability measure on $C^0(\overline{\Omega})$, and let $P : \theta \in C^0(\overline{\Omega}) \mapsto \sigma \in U$ be defined as P_1 or P_2 in section 2.3. Then, the function $\Phi^0 : C^0(\overline{\Omega}) \times \mathbb{R}^{JL} \rightarrow \mathbb{R}$ defined in (12), with $G^0 = F^0 \circ P : C^0(\overline{\Omega}) \rightarrow \mathbb{R}^{JL}$, satisfies assumptions 1–3 of Theorem 2. If $P = P_2$, then also assumption 4 of Theorem 2 is satisfied. If $P = P_1$, assumption 4 holds if*

$$(22) \quad \beta_{\|\cdot\|_{L^\infty(\Omega)}}^2 \alpha_{\|\cdot\|_{L^\infty(\Omega)}}^{-1} \in L^2_{\mu_{pr}}(C^0(\overline{\Omega})).$$

Proof. Let σ be an admissible functions in U . We have that

$$\begin{aligned} \|F^0(\sigma)\|_{C_\zeta} &\leq C \sum_{j=1}^J \sum_{l=1}^L \left| \langle \Lambda_{A_\sigma^0} g_l, \phi_j \rangle_{H^{-1/2}(\partial\Omega), H^{1/2}(\partial\Omega)} \right| \\ &\leq C \sup_l \|\Lambda_{A_\sigma^0} g_l\|_{H^{-1/2}(\partial\Omega)} \sup_j \|\phi_j\|_{H^{1/2}(\partial\Omega)} \\ &\leq C \beta_{[\sigma^-, \sigma^+]}^2 \alpha_{[\sigma^-, \sigma^+]}^{-1} \sup_l \|g_l\|_{H^{1/2}(\partial\Omega)} \\ &\leq C \beta_{[\sigma^-, \sigma^+]}^2 \alpha_{[\sigma^-, \sigma^+]}^{-1}. \end{aligned}$$

If $P = P_1$, then $\sigma = \exp(\theta)$, where $\theta \in C^0(\bar{\Omega})$, and $\beta_{[\sigma^-, \sigma^+]}^2 \alpha_{[\sigma^-, \sigma^+]}^{-1}$ is a positive and monotonic nondecreasing function of $\|\theta\|_{L^\infty(\Omega)}$ (see (14)). Thus we obtain

$$\|G^0(\theta)\|_{C_\zeta} \leq \beta_{\|\theta\|_{L^\infty(\Omega)}}^2 \alpha_{\|\theta\|_{L^\infty(\Omega)}}^{-1}.$$

If $P = P_2$, $\|G^0(\theta)\|_{C_e}$ is bounded by a constant $\forall \theta \in C^0(\bar{\Omega})$ since P_2 is uniformly bounded. Using the triangle inequality we have that

$$\Phi^0(\theta, z) \leq C (\|z\|_{C_e}^2 + \|G^0(\theta)\|_{C_e}^2),$$

and therefore assumption 1 follows. To fulfill assumption 3 we note that we have

$$\begin{aligned} |\Phi^0(\theta, z_1) - \Phi^0(\theta, z_2)| &= \frac{1}{2} |\langle z_1 + z_2 - 2G^0(\theta), z_1 - z_2 \rangle_{C_e}| \\ &\leq C(\|z_1\|_{C_e} + \|z_2\|_{C_e} + 2\|G^0(\theta)\|_{C_e}) \|z_1 - z_2\|_{C_e}. \end{aligned}$$

Let r such that $\max\{\|z_1\|_{C_e}, \|z_2\|_{C_e}\} < r$. Hence we obtain

$$\begin{aligned} |\Phi^0(\theta, z_1) - \Phi^0(\theta, z_2)| &\leq C(2r + 2\|G^0(\theta)\|_{C_e}) \|z_1 - z_2\|_{C_e} \\ &\leq M(r, \|\theta\|_{L^\infty(\Omega)}) \|z_1 - z_2\|_{C_e} \end{aligned}$$

with

$$M(r, \|\theta\|_{L^\infty(\Omega)}) = C(2r + 2\|G^0(\theta)\|_{C_e}).$$

If $P = P_2$, $M(r, \|\theta\|_{L^\infty(\Omega)})$ is positive and monotonic nondecreasing and uniformly bounded with respect to $\|\theta\|_{L^\infty(\Omega)}$. Hence, assumptions 3 and 4 follow. In the case $P = P_1$ we have that

$$M(r, \|\theta\|_{L^\infty(\Omega)}) = C \left(2r + 2\beta_{\|\theta\|_{L^\infty(\Omega)}}^2 \alpha_{\|\theta\|_{L^\infty(\Omega)}}^{-1} \right).$$

We note that $M(r, \|\theta\|_{L^\infty(\Omega)})$ is positive and monotonic nondecreasing, hence assumption 3 follows. Moreover if

$$\beta_{\|\cdot\|_{L^\infty(\Omega)}}^2 \alpha_{\|\cdot\|_{L^\infty(\Omega)}}^{-1} \in L^2_{\mu_{pr}}(C^0(\bar{\Omega})) ,$$

then

$$M(r, \|\cdot\|_{L^\infty(\Omega)}) \in L^2_{\mu_{pr}}(C^0(\bar{\Omega})) .$$

Hence assumption 4 of Theorem 2 is satisfied and μ^0 is Lipschitz in the data z with respect to the Hellinger distance. Indeed we can observe that given z_1, z_2 such that $\max\{\|z_1\|_{C_e}, \|z_2\|_{C_e}\} < r$, the two corresponding measures $\mu^0(\theta|z_1)$ and $\mu^0(\theta|z_2)$ satisfy

$$\begin{aligned} 2d_{Hell}^2(\mu^0(\theta|z_1), \mu^0(\theta|z_2)) &\leq C \int_{C^0(\bar{\Omega})} (2\|z\|_{C_e} + 2\|G^0(\theta)\|_{C_e})^2 \|z_1 - z_2\|_{C_e}^2 \mu_{pr}(d\theta) \\ &\leq C \int_{C^0(\bar{\Omega})} \left(2r + 2\beta_{\|\theta\|_{L^\infty(\Omega)}}^2 \alpha_{\|\theta\|_{L^\infty(\Omega)}}^{-1}\right)^2 \|z_1 - z_2\|_{C_e}^2 \mu_{pr}(d\theta) , \end{aligned}$$

and hence Lipschitz continuity follows if $\beta_{\|\cdot\|_{L^\infty(\Omega)}}^2 \alpha_{\|\cdot\|_{L^\infty(\Omega)}}^{-1} \in L^2_{\mu_{pr}}(C^0(\bar{\Omega}))$.

It remains to show that assumption 2 is also satisfied. Assume that $P = P_1$. If $\|\theta - \theta_n\|_{L^\infty(\Omega)} \rightarrow 0$, then $P(\theta_n) \rightarrow P(\theta)$ uniformly. Then by Lemma 3 we have that $G^0 = F^0 \circ P$ is continuous at θ . Assume now $P = P_2$. If $\|\theta - \theta_n\|_{L^\infty(\Omega)} \rightarrow 0$, then by Proposition 1 $P(\theta_n) \rightarrow P(\theta)$ in $L^q(\Omega)$, $1 \leq q < \infty$, at the points where the level sets have measure zero. However, since we are assuming $\theta \sim \mu_{pr}$ and μ_{pr} is a Gaussian probability measure on $C^0(\bar{\Omega})$, it follows from Proposition 1 that θ has μ_{pr} -almost surely this property. Finally since $P_2(\theta_n(x))$ is uniformly bounded for all $x \in \bar{\Omega}$ and all $n > 0$, by Lemma 2 we have that assumption 2 is satisfied also in the case where $P = P_2$. ■

Remark 3. The result in Lemma 2 can be proved in a similar way also for the sequence $\{\Lambda_{A_{\sigma_n}^\varepsilon} g\}_{n>0}$. It can also be proved that when $P = P_1$ also for $G^\varepsilon(\theta)$ we have that

$$\|G^\varepsilon(\theta)\|_{C_e} \leq C \beta_{\|\theta\|_{L^\infty(\Omega)}}^2 \alpha_{\|\theta\|_{L^\infty(\Omega)}}^{-1} ,$$

while when $P = P_2$, $\|G^\varepsilon(\theta)\|_{C_e}$ is bounded by a constant independent of θ . Hence, under the assumptions of Theorem 3 the posterior measure (8) based on the potential function Φ^ε is also well-defined and Lipschitz continuous in the data with respect to the Hellinger distance.

4.2. Homogenization error and convergence analysis. Before moving to the numerical aspects of the problem, an investigation of the validity of our approach is necessary. First we observe that (6) can be rewritten as

$$(23) \quad z = F^0(\sigma^*) + \underbrace{(F^\varepsilon(\sigma^*) - F^0(\sigma^*))}_{m(\sigma^*)} + e, \quad e \sim \mathcal{N}(0, C_e) .$$

The quantity $m(\sigma^*)$ represents the homogenization error capturing the mismatch between the full multiscale model and the homogenized one. In particular, (23) suggests that the observed data originating from the full multiscale model can be seen as data originating from the homogenized model, which are affected by two sources of errors: the noise and

the homogenization error. Both sources of errors can affect our predictions and we must take them into account when solving inverse problems to obtain good approximations of the unknown, especially when ε is relatively large. For the homogenization error we can show that we have in our case that $m(\sigma) \rightarrow 0$ as $\varepsilon \rightarrow 0$ for every $\sigma \in U$, as stated in the following theorem.

Theorem 4. *Let $\sigma \in U$, and let $\{A_\sigma^\varepsilon\}_{\varepsilon>0}$ be a sequence of matrices in $M(\alpha_{[\sigma^-, \sigma^+]}, \beta_{[\sigma^-, \sigma^+]}, \Omega)$ which G-converges to the matrix $A_\sigma^0 \in M(\alpha_{[\sigma^-, \sigma^+]}, \beta_{[\sigma^-, \sigma^+]}, \Omega)$, and let $m(\sigma) = \text{vec}(\{\tilde{m}_{jl}(\sigma)\}_{\substack{1 \leq j \leq J \\ 1 \leq l \leq L}})$, where*

$$\tilde{m}_{jl}(\sigma) = \langle (\Lambda_{A_\sigma^\varepsilon} - \Lambda_{A_\sigma^0})g_l, \phi_j \rangle_{H^{-1/2}(\partial\Omega), H^{1/2}(\partial\Omega)}, \quad j = 1, \dots, J, l = 1, \dots, L,$$

where $\Gamma_j \subset \partial\Omega \forall j = 1, \dots, L$, $\Gamma_i \cap \Gamma_j = \emptyset$ for $i \neq j$, and $\phi_j, g_l \in H^{1/2}(\partial\Omega) \forall j = 1, \dots, J$, $\text{supp}(\phi_j) \subseteq \Gamma_j \forall j = 1, \dots, J$. Then $\|m(\sigma)\|_{C_e} \rightarrow 0$ as $\varepsilon \rightarrow 0$.

Proof. We have that for arbitrary j and l and $\forall \sigma \in U$

$$|\tilde{m}_{jl}(\sigma)| = |\langle (\Lambda_{A_\sigma^\varepsilon} - \Lambda_{A_\sigma^0})g_l, \phi_j \rangle_{H^{-1/2}(\partial\Omega), H^{1/2}(\partial\Omega)}|.$$

Using integration by parts we have that

$$(24) \quad |\tilde{m}_{jl}(\sigma)| = \left| \int_{\Omega} (A_\sigma^\varepsilon \nabla u^\varepsilon - A_\sigma^0 \nabla u^0) \cdot \nabla \tilde{\phi}_j \, dx \right|,$$

where $\tilde{\phi}_j$ is some function in $H^1(\Omega)$ whose trace is ϕ_j . From G-convergence of A_σ^ε to A_σ^0 we know that (24) converges to zero as $\varepsilon \rightarrow 0$. ■

Theorem 5. *Let μ^ε and μ^0 be defined as in (8) and (13), respectively. Let the assumptions of Theorem 3 be satisfied, together with (22). Then we have that*

$$\lim_{\varepsilon \rightarrow 0} d_{Hell}(\mu^0, \mu^\varepsilon) = 0.$$

Proof. From the definition of the Hellinger distance we have that

$$(25) \quad \begin{aligned} 2d_{Hell}^2(\mu^0, \mu^\varepsilon) &= \int_{C^0(\bar{\Omega})} \left(\sqrt{\frac{d\mu^0}{d\mu_{pr}}} - \sqrt{\frac{d\mu^\varepsilon}{d\mu_{pr}}} \right)^2 \mu_{pr}(d\theta) \\ &= \int_{C^0(\bar{\Omega})} \left(\frac{1}{\sqrt{K^0}} \exp\left(-\frac{1}{2}\Phi^0(\theta, z)\right) - \frac{1}{\sqrt{K^\varepsilon}} \exp\left(-\frac{1}{2}\Phi^\varepsilon(\theta, z)\right) \right)^2 \mu_{pr}(d\theta), \end{aligned}$$

where K^0 and K^ε are the two normalization constants such that $\mu^0(\theta|z)$ and $\mu^\varepsilon(\theta|z)$ are probability measures, i.e.,

$$K^0 = \int_{C^0(\bar{\Omega})} \exp(-\Phi^0(\theta, z)) \mu_{pr}(d\theta), \quad K^\varepsilon = \int_{C^0(\bar{\Omega})} \exp(-\Phi^\varepsilon(\theta, z)) \mu_{pr}(d\theta).$$

Let us notice that

$$\begin{aligned} |K^0 - K^\varepsilon| &\leq \int_{C^0(\bar{\Omega})} |\exp(-\Phi^0(\theta, z)) - \exp(-\Phi^\varepsilon(\theta, z))| \mu_{pr}(d\theta) \\ (26) \quad &\leq \int_{C^0(\bar{\Omega})} |\Phi^0(\theta, z) - \Phi^\varepsilon(\theta, z)| \mu_{pr}(d\theta). \end{aligned}$$

From (25) we get that

$$2d_{Hell}^2(\mu^0, \mu^\varepsilon) \leq I_1 + I_2,$$

where

$$\begin{aligned} I_1 &= \frac{1}{K^0} \int_{C^0(\bar{\Omega})} \left(\exp\left(-\frac{1}{2}\Phi^0(\theta, z)\right) - \exp\left(-\frac{1}{2}\Phi^\varepsilon(\theta, z)\right) \right)^2 \mu_{pr}(d\theta), \\ I_2 &= \left(\frac{1}{\sqrt{K^0}} - \frac{1}{\sqrt{K^\varepsilon}} \right)^2 K^\varepsilon. \end{aligned}$$

We have that

$$I_1 \leq \frac{1}{4K^0} \int_{C^0(\bar{\Omega})} (\Phi^0(\theta, z) - \Phi^\varepsilon(\theta, z))^2 \mu_{pr}(d\theta)$$

and

$$\begin{aligned} I_2 &\leq \frac{1}{4} \max \{(K^0)^{-3}, (K^\varepsilon)^{-3}\} (K^0 - K^\varepsilon)^2 \\ &\leq C \int_{C^0(\bar{\Omega})} (\Phi^0(\theta, z) - \Phi^\varepsilon(\theta, z))^2 \mu_{pr}(d\theta), \end{aligned}$$

where we have used (26). Using the definition of Φ^0 and Φ^ε we find

$$\begin{aligned} 2d_{Hell}^2(\mu^0, \mu^\varepsilon) &\leq C \int_{C^0(\bar{\Omega})} (\Phi^0(\theta, z) - \Phi^\varepsilon(\theta, z))^2 \mu_{pr}(d\theta) \\ &\leq C \int_{C^0(\bar{\Omega})} (2\|z\|_{C_e} + \|G^0(\theta)\|_{C_e} + \|G^\varepsilon(\theta)\|_{C_e})^2 \|G^0(\theta) - G^\varepsilon(\theta)\|_{C_e}^2 \mu_{pr}(d\theta). \end{aligned}$$

From Theorem 4 we have that $\lim_{\varepsilon \rightarrow 0} \|G^0(\theta) - G^\varepsilon(\theta)\|_{C_e} = 0$. We also have that (see Theorem 3) if $P = P_1$ both $\|G^0(\theta)\|_{C_e}$ and $\|G^\varepsilon(\theta)\|_{C_e}$ are bounded by some scalar multiple of $\beta_{\|\theta\|_{L^\infty(\Omega)}}^2 \alpha_{\|\theta\|_{L^\infty(\Omega)}}^{-1}$ which is square integrable with respect to μ_{pr} . Otherwise if $P = P_2$ both $\|G^0(\theta)\|_{C_e}$ and $\|G^\varepsilon(\theta)\|_{C_e}$ are bounded by a constant since P_2 is uniformly bounded, and again square integrability follows. Then by the Lebesgue's dominated convergence theorem it follows that $d_{Hell}(\mu^0, \mu^\varepsilon) \rightarrow 0$ as $\varepsilon \rightarrow 0$. ■

The interpretation of the result is that when ε is small we can neglect the homogenization error, since it will be close to zero, and we do not need to take into account its probability distribution in the inversion process. However, for larger values of ε , the mismatch between the observations and the data produced by the homogenized model might not be negligible, and using the coarse grained approach without taking into account the homogenization error distribution may lead to bad predictions. In order to avoid that, we can correct the likelihood function, by approximating the probability distribution of the homogenization error. In [9] a strategy for approximating the first two moments of the distribution of the discretization error caused by the FEM is proposed. Hence, by following [9], we derive an algorithm which aims at approximating the mean \bar{m} and the covariance C_m of the homogenization error distribution.

We assume a Gaussian distribution for the homogenization error, so that $m \sim \mathcal{N}(\bar{m}, C_m)$ $\forall \sigma$, and we can rewrite (23) as

$$(27) \quad z = F^0(\sigma^*) + e, \quad e \sim \mathcal{N}(\bar{m}, C_e + C_m).$$

The assumption of the homogenization error being Gaussian allows us to exploit the Gaussian assumption on the noise distribution, hence to simplify the theoretical and numerical treatment of the corrected posterior. We still lack a theoretical result to support this assumption, which remains a topic for further investigations. We note that a one-dimensional result in this direction has been established in [22]. As illustrated in Algorithm 1, the homogenization error distribution is approximated offline. Only M evaluations of the full multiscale model are needed. Hence, we use this approximation to modify the potential function as in (28) and sample from the posterior by evaluating only the coarse homogenized model. We note that in (27) to apply the Bayesian framework for inverse problem, we still assume the independence of e and θ , despite the introduction of the homogenization error in e . Nevertheless, the practical usefulness of such an algorithm has been shown in numerous works (see [6, 9]). Then, we may define the new likelihood as

$$(28) \quad \Phi^0(\theta, \bar{z}) = \frac{1}{2} \|\bar{z} - G^0(\theta)\|_{C_e + C_m}^2,$$

where $\bar{z} = z - \bar{m}$. Note that conclusions about existence and well-posedness of the posterior measure are still valid under this definition of the potential function, which is equivalent to the one in (12), apart from the fact that observations z are shifted by \bar{m} , and the covariance matrix is given by $C_e + C_m$.

Algorithm 1. Approximation of homogenization error distribution.

input : prior measure, sample size M , map $P : \theta \mapsto \sigma$
output: mean \bar{m} and covariance C_m of the homogenization error

- 1 Draw from the prior measure a sample of realizations $S = \{\theta_1, \dots, \theta_M\}$
 - 2 **for** $i = 1, \dots, M$ **do**
 - 3 $| m_i = G^\varepsilon(\theta_i) - G^0(\theta_i) = F^\varepsilon(P(\theta_i)) - F^0(P(\theta_i))$
 - 4 **end**
 - 5 $\bar{m} = \frac{1}{M} \sum_{i=1}^M m_i$ $C_m = \frac{1}{M} \sum_{i=1}^M (\bar{m} - m_i)(\bar{m} - m_i)^\top$
-

5. Numerical approximation of the posterior density. The output of the Bayesian approach consists in the posterior measure. However, in practice numerical sampling is needed to approximate the distribution, in order to obtain some meaningful information (such as expected value or variance of the unknown, or confidence intervals). We consider as prior a Gaussian measure $\mu_{pr} = \mathcal{N}(\theta_{pr}, C_{pr})$ on the Hilbert space $L^2(\Omega)$. The random variable $\theta \sim \mathcal{N}(\theta_{pr}, C_{pr})$ can be written using the Karhunen–Loëve expansion as

$$\theta(x) = \theta_{pr}(x) + \sum_{k=1}^{\infty} \sqrt{\lambda_k} \eta_k \varphi_k(x),$$

where $\{\varphi_k, \lambda_k\}_{k=1}^{\infty}$ is an orthonormal set of eigenfunctions and eigenvalues of C_{pr} , and $\{\eta_k\}_{k=1}^{\infty}$ is an independent and identically distributed (i.i.d.) sequence with $\eta_1 \sim \mathcal{N}(0, 1)$. Since we defined the push forward maps as $P_i : C^0(\bar{\Omega}) \rightarrow U$, $i = 1, 2$, we may ask which condition the prior measure has to satisfy so that each sample from μ_{pr} is in $C^0(\bar{\Omega})$. For the Matérn covariance operator that we will use in the numerical examples, we will ensure that draws from $\mathcal{N}(\theta_{pr}, C_{pr})$ are continuous (see section 7.1).

In numerical experiments to reduce the dimension of the unknown we use a truncated Karhunen–Loëve expansion

$$\theta^K(x) = \theta_{pr}(x) + \sum_{k=1}^K \sqrt{\lambda_k} \eta_k \varphi_k(x),$$

where $\{\varphi_k, \lambda_k\}_{k=1}^K$ is the orthonormal set of eigenfunctions and eigenvalues of C_{pr} corresponding to the K largest eigenvalues. The unknown parameter is then parameterized by the K coefficients $\{\eta_k\}_{k=1}^K$, which are a priori i.i.d. as $\mathcal{N}(0, 1)$. In what follows, we will denote sometimes the unknown parameter as $\theta_{\boldsymbol{\eta}}^K$ to emphasize its dependence on $\boldsymbol{\eta} = (\eta_1, \dots, \eta_K)^{\top}$. Hence, the inverse problem consists in approximating the posterior distribution of the K coefficients by sampling from the posterior density $\pi^0(\boldsymbol{\eta}|z)$ which is given by

$$(29) \quad \pi^0(\boldsymbol{\eta}|z) \propto \exp\left(-\frac{1}{2}\|z - G^0(\theta_{\boldsymbol{\eta}}^K)\|_{C_{\zeta}}^2 - \frac{1}{2}\|\theta_{\boldsymbol{\eta}}^K - \theta_{pr}\|_{C_{pr}}^2\right),$$

where $\|\cdot\|_{C_{pr}}$ is the norm induced by the scalar product

$$\langle \cdot, \cdot \rangle_{C_{pr}} = \left\langle C_{pr}^{-1/2}(\cdot), C_{pr}^{-1/2}(\cdot) \right\rangle_{L^2(\Omega)},$$

and for any $\theta \in L^2(\Omega)$ and any $\alpha \in \mathbb{R}$ we have that

$$C_{pr}^{\alpha}(\theta) = \sum_{k=1}^{\infty} \lambda_k^{\alpha} \langle \theta, \varphi_k \rangle_{L^2(\Omega)} \varphi_k.$$

It is easy to obtain that (29) reduces to

$$(30) \quad \pi^0(\boldsymbol{\eta}|z) \propto \exp\left(-\frac{1}{2}\|z - G^0(\theta_{\boldsymbol{\eta}}^K)\|_{C_{\zeta}}^2 - \frac{1}{2}\boldsymbol{\eta}^{\top} \boldsymbol{\eta}\right).$$

To sample from the posterior density we employ the MCMC techniques. Many algorithms belonging to the family of MCMC sampling methods are available in the literature. We decided to use the Metropolis–Hastings (MH) algorithm, which we illustrate just below. With this approach at each iteration we generate a new candidate $\boldsymbol{\eta} \in \mathbb{R}^K$ from a proposal density

$q(\boldsymbol{\eta}^j, \boldsymbol{\eta})$, $q : \mathbb{R}^K \times \mathbb{R}^K \rightarrow \mathbb{R}^+$, where $\boldsymbol{\eta}^j$ is the current value of the variable. This new candidate is accepted with probability

$$(31) \quad a(\boldsymbol{\eta}^j, \boldsymbol{\eta}) = \min \left\{ 1, \frac{\pi^0(\boldsymbol{\eta}|z)q(\boldsymbol{\eta}, \boldsymbol{\eta}^j)}{\pi^0(\boldsymbol{\eta}^j|z)q(\boldsymbol{\eta}^j, \boldsymbol{\eta})} \right\}.$$

Otherwise the candidate is rejected and the chain remains at the current position $\boldsymbol{\eta}^j$. Note that if the proposal density is symmetric, i.e., $q(\boldsymbol{\eta}^j, \boldsymbol{\eta}) = q(\boldsymbol{\eta}, \boldsymbol{\eta}^j)$, (31) reduces to

$$a(\boldsymbol{\eta}^j, \boldsymbol{\eta}) = \min \left\{ 1, \frac{\pi^0(\boldsymbol{\eta}|z)}{\pi^0(\boldsymbol{\eta}^j|z)} \right\}.$$

In our experiments we consider the random walk proposal distribution to explore the density. Then

$$(32) \quad q(\boldsymbol{\eta}^j, \boldsymbol{\eta}) = \frac{1}{\sqrt{(2\pi s^2)^K}} \exp \left(-\frac{1}{2s^2} (\boldsymbol{\eta} - \boldsymbol{\eta}^j)^\top (\boldsymbol{\eta} - \boldsymbol{\eta}^j) \right),$$

which is symmetric and leads to Algorithm 2. The approximation of the target distribution improves as the number of samples N_{sample} increases, and asymptotic convergence is guaranteed as $N_{sample} \rightarrow \infty$ under certain regularity properties of the target distribution and the proposal density. Therefore, the results may be strongly dependent on the number of samples required, but also on the proposal density. In particular, it is a difficult task to establish when a sample is large enough. At the same time, another general issue for the MH algorithm is the choice of s in (32), whose magnitude affects the speed at which the posterior distribution is explored and the number of rejected realizations.

Algorithm 2. Metropolis–Hastings algorithm.

```

input : posterior density  $\pi^0$ , starting point  $\boldsymbol{\eta}^1 \in \mathbb{R}^K$ , number of samples desired
          $N_{sample}$ , symmetric proposal density  $\mathcal{N}(0, s^2 I)$ 
output: sample of realization  $\mathcal{S} \in \mathbb{R}^{K \times N_{sample}}$ 

1 Initialization:  $j = 1$ ,  $\mathcal{S} = \boldsymbol{\eta}^1$ 
2 while  $j < N_{sample}$  do
3    $\boldsymbol{\eta} = \boldsymbol{\eta}^j + sw$ ,  $w \sim \mathcal{N}(0, I)$ 
4    $a(\boldsymbol{\eta}^j, \boldsymbol{\eta}) = \min \left\{ 1, \frac{\pi^0(\boldsymbol{\eta}|z)}{\pi^0(\boldsymbol{\eta}^j|z)} \right\}$ 
5   Draw  $u \sim \mathcal{U}([0, 1])$ 
6   if  $a(\boldsymbol{\eta}^j, \boldsymbol{\eta}) > u$  then
7     | accept:  $\boldsymbol{\eta}^{j+1} = \boldsymbol{\eta}$ 
8   else
9     | reject:  $\boldsymbol{\eta}^{j+1} = \boldsymbol{\eta}^j$ 
10  end
11   $\mathcal{S} = \mathcal{S} \cup \boldsymbol{\eta}^{j+1}$ ,  $j = j + 1$ 
12 end

```

6. Numerical approximation of the forward model. At each MH iteration we need to evaluate $\pi^0(\boldsymbol{\eta}|z)$, where $\boldsymbol{\eta}$ is a new candidate point, and π^0 is the posterior density given in (30). Hence, given $\sigma = P(\theta_{\boldsymbol{\eta}}^K)$, where $P : C^0(\bar{\Omega}) \rightarrow U$ is one of two maps introduced in section 2.3, what remains to be discussed is how to evaluate $F^0(\sigma)$. The procedure can be substantially split into two parts:

1. Solve for each $l = 1, \dots, L$,

$$(33) \quad \begin{aligned} -\nabla \cdot (A_\sigma^0 \nabla u^0) &= 0 && \text{in } \Omega, \\ u^0 &= g_l && \text{on } \partial\Omega, \end{aligned}$$

where A_σ^0 is the homogenized tensor corresponding to $A_\sigma^\varepsilon(x) = A(\sigma(x), x/\varepsilon)$.

2. Approximate the boundary fluxes, and evaluate (11).

6.1. Numerical homogenization. Since given A_σ^ε the analytic solution for the corresponding A_σ^0 is often not known, numerical homogenization is needed. We employ the finite element heterogeneous multiscale method (FE-HMM), which approximates the homogenized problem originating from (9) taking as input only the multiscale data. For a detailed analysis about the FE-HMM we refer to [1, 2]. We state here the simplest version involving only piecewise linear macro- and microsimplicial elements. The method is based on a macro finite element space

$$S^1(\Omega, \mathcal{T}_H) = \left\{ v^H \in H^1(\Omega) : v^H|_K \in \mathcal{P}^1(K) \ \forall K \in \mathcal{T}_H \right\},$$

where \mathcal{T}_H is a partition of Ω in simplicial elements K of diameter H_K , and $\mathcal{P}^1(K)$ is the space of linear polynomials on K . Then, the homogenized tensor is approximated at each integration point by solving a micro problem on a sampling domain $K_\delta = x_K + (-\delta/2, \delta/2)^d$, with $\delta \geq \varepsilon$. For a sampling domain K_δ , we define a micro finite element space

$$S^1(K_\delta, \mathcal{T}_h) = \left\{ v^h \in W(K_\delta) : v^h|_T \in \mathcal{P}^1(T) \ \forall T \in \mathcal{T}_h \right\},$$

where

$$W(K_\delta) = W_{per}^1 = \left\{ v \in H_{per}^1(K_\delta) : \int_{K_\delta} v \, dx = 0 \right\}.$$

Let u_l^H be the approximate solution to problem (33). The numerical method reads as follows: find $u_l^H \in S^1(\Omega, \mathcal{T}_H)$, $u_l^H = g_l$ on $\partial\Omega$, such that

$$B_H(u_l^H, v^H) = 0 \quad \forall v^H \in S_0^1(\Omega, \mathcal{T}_H),$$

where $S_0^1(\Omega, \mathcal{T}_H) = S^1(\Omega, \mathcal{T}_H) \cap H_0^1(\Omega)$, and

$$(34) \quad B_H(v^H, w^H) = \sum_{K \in \mathcal{T}_H} \frac{|K|}{|K_\delta|} \int_{K_\delta} A_\sigma^\varepsilon(x) \nabla v_K^h \cdot \nabla w_K^h \, dx.$$

In (34) v_K^h (respectively, w_K^h) denotes the solution to the micro problem: find v_K^h such that $v_K^h - v^H \in S^1(K_\delta, \mathcal{T}_h)$ and

$$(35) \quad \int_{K_\delta} A_\sigma^\varepsilon(x) \nabla v_K^h \cdot \nabla z^h \, dx = 0 \quad \forall z^h \in S^1(K_\delta, \mathcal{T}_h).$$

Note that since $A_\sigma^\varepsilon = A(\sigma(x), x/\varepsilon)$ admits scale separation and is periodic in the second variable, we collocate the slow variable at the macro quadrature points x_K , by replacing $A_\sigma^\varepsilon(x)$ with $A(\sigma(x_K), x/\varepsilon)$ in (34), (35).

6.2. Model order reduction. The main cost of the FE-HMM comes from the repeated solution of cell problems, whose number increases as we refine the macro mesh to obtain an appropriate approximation of the homogenized solution. This is particularly undesirable when solving inverse problems, since by using, e.g., the MH algorithm, one needs multiple evaluations of the likelihood function for different realizations of the parameter of interest. We therefore combine the reduced basis methodology with the FE-HMM to drastically reduce the computational effort. For a detailed description and analysis of the method, that is, the RB-FE-HMM, we mention [3]. The main idea is the following. During what is called the *offline stage*, we select a small number, i.e., N , of carefully precomputed micro solutions to construct a small subspace of microscopic functions which we call $S^N(Y)$. Then, in the *online stage*, we use these precomputed solutions to obtain fast evaluations of the homogenized tensor at the macroscopic quadrature points. The basis of $S^N(Y)$ is selected by using a greedy procedure. Let us note that if we map the domain K_δ into the reference domain $Y = (0, 1)^d$ through $x = G_{x_K}(y) = x_K + \delta(y - 1/2)$, we can define

$$B_H(v^H, w^H) = \sum_{K \in \mathcal{T}_H} |K| A^{0,h}(\sigma(x_K)) \nabla v^H(x_K) \cdot \nabla w^H(x_K)$$

with

$$A_{ij}^{0,h}(\sigma(x_K)) = \int_Y A(\sigma(x_K), y) \left(\mathbf{e}^i - \nabla \chi_K^{i,\hat{h}} \right) \cdot \left(\mathbf{e}^j - \nabla \chi_K^{j,\hat{h}} \right) \, dy,$$

where $\hat{h} = h/\delta$, and $\chi_K^{i,\hat{h}} \in S^1(Y, \mathcal{T}_{\hat{h}})$ (respectively, $\chi_K^{j,\hat{h}}$) is the solution of the micro problem

$$(36) \quad \int_Y A(\sigma(x_K), y) \nabla \chi_K^{i,\hat{h}} \cdot \nabla z^{\hat{h}} \, dy = \int_Y A(\sigma(x_K), y) \mathbf{e}^i \cdot \nabla z^{\hat{h}} \, dy \quad \forall z^{\hat{h}} \in S^1(Y, \mathcal{T}_{\hat{h}}).$$

It can be shown [3] that

$$\frac{1}{|K_\delta|} \int_{K_\delta} A(\sigma(x_K), x/\varepsilon) \nabla v_K^h \cdot \nabla w_K^h \, dx = A^{0,h}(\sigma(x_K)) \nabla v^H(x_K) \cdot \nabla w^H(x_K).$$

Since each micro problem is parameterized by the value $\sigma(x_K)$ we can think to apply model order reduction to speed up the computation. We define the space of parameters $\Xi = [\sigma^-, \sigma^+] \times \{1, \dots, d\}$. For a given $\xi = (t, i) \in \Xi$, we denote the corresponding micro solution as $\chi_\xi^{\hat{h}}$ which satisfies

$$b\left(\chi_\xi^{\hat{h}}, z^{\hat{h}}; \xi\right) = f\left(z^{\hat{h}}; \xi\right) \quad \forall z^{\hat{h}} \in S^1(Y, \mathcal{T}_{\hat{h}}),$$

where

$$b(z^{\hat{h}}, w^{\hat{h}}; \xi) = \int_Y A(t, y) \nabla z^{\hat{h}} \cdot \nabla w^{\hat{h}} dy,$$

and

$$f(z^{\hat{h}}; \xi) = \int_Y A(t, y) \mathbf{e}^i \cdot \nabla z^{\hat{h}}.$$

To construct the reduced space $S^N(Y)$, we randomly define a training set $\Xi_{Train} \subset \Xi$,

$$\Xi_{Train} = \{\xi_n = (t_n, i_n) : 1 \leq n \leq N_{Train}, t_n \in [\sigma^-, \sigma^+], 1 \leq i_n \leq d\}.$$

To select the micro problems in the offline stage, we randomly draw one element from Ξ_{Train} , i.e., ξ_1 , and we compute the first basis function by solving the micro problem: find $\chi_{\xi_1}^{\hat{h}} \in S^1(Y, \mathcal{T}_{\hat{h}})$ such that

$$b(\chi_{\xi_1}^{\hat{h}}, z^{\hat{h}}; \xi_1) = f(z^{\hat{h}}; \xi_1) \quad \forall z^{\hat{h}} \in S^1(Y, \mathcal{T}_{\hat{h}}).$$

We define

$$\psi_1^{\hat{h}} = \frac{\chi_{\xi_1}^{\hat{h}}}{\|\chi_{\xi_1}^{\hat{h}}\|_{W_{per}^1(Y)}},$$

and we initialize the space $S^1(Y) = \text{span}\{\psi_1^{\hat{h}}\}$. Thus, we continue to add new basis functions to $S^1(Y)$ until convergence of an a posteriori error indicator below a certain tolerance. The output of the offline stage is then the reduced space

$$S^N(Y) = \text{span}\{\psi_1^{\hat{h}}, \dots, \psi_N^{\hat{h}}\}.$$

An efficient way to both implement the greedy algorithm and compute the residuals for the a posteriori error control is crucial. An important assumption is that for a given $t_n \in [\sigma^-, \sigma^+]$, the tensor $A(t_n, y)$ is available in the affine form

$$(37) \quad A(t_n, y) = \sum_{q=1}^Q \Theta_q(t_n) A_q(y) \quad \forall y \in Y,$$

where $\Theta_q : [\sigma^-, \sigma^+] \rightarrow \mathbb{R}$, $q = 1, \dots, Q$. In case the tensor is not directly available in the form (37), a greedy algorithm, called the empirical interpolation method (EIM), can be applied to obtain an affine approximation of the tensor [17]. Once $S^N(Y)$ has been constructed, we can then define a macro method similar to the FE-HMM, to obtain an approximation of the solution of (33). The method reads, Find $u_l^{H,RB} \in S^1(\Omega, \mathcal{T}_H)$, $u_l^{H,RB} = g_l$ on $\partial\Omega$, such that

$$(38) \quad B_{H,RB}(u_l^{H,RB}, v^H) = 0 \quad \forall v^H \in S_0^1(\Omega, \mathcal{T}_H),$$

where

$$(39) \quad B_{H,RB}(v^H, w^H) = \sum_{K \in \mathcal{T}_H} |K| A^{0,N}(\sigma(x_K)) \nabla v^H(x_K) \cdot w^H(x_K),$$

and

$$A_{ij}^{0,N}(\sigma(x_K)) = \int_Y A(\sigma(x_K), y) \left(\mathbf{e}^i - \nabla \chi_K^{i,N} \right) \cdot \left(\mathbf{e}^j - \nabla \chi_K^{j,N} \right) dy.$$

The function $\chi_K^{i,N}$ is the solution of (36) in the reduced basis space. Thanks to the affine representation of the tensor A_σ^ϵ , solving the micro problems in the reduced space consists in solving a small $N \times N$ linear system, which leads to a significant computational speed-up compared to classical numerical homogenization [3]. The size N of the reduced space is problem dependent and relies on the decay of the numerical error introduced by the reduced basis methodology which can be quantified by means of the notion of Kolmogorov N -width (see Remark 5). In practice such an error often exhibits an exponential decay.

6.3. Approximate boundary flux computation. Once the approximated solution of (33) has been computed, what is left is to evaluate the boundary fluxes to obtain the values defined through (11). To do so, we employ a method based on a Galerkin projection, which we have introduced and analyzed in [4]. For completeness, we briefly illustrate the algorithm. We assume the domain Ω to be a polygonal domain. We suppose that the approximate flux at the corners of Ω is specified from direct calculation with the given Dirichlet data (see [10] for details). We next introduce the following subspace of $S^1(\Omega, \mathcal{T}_H)$:

$$S_c^1(\Omega, \mathcal{T}_H) = \{v^H \in S^1(\Omega, \mathcal{T}_H) : v^H = 0 \text{ at the corners of } \Omega\}.$$

Let us denote as $S^1(\partial\Omega, \mathcal{T}_H)$ the finite dimensional space of functions which are restrictions on the boundary of functions in $S_c^1(\Omega, \mathcal{T}_H)$. Suppose we have computed the approximate solutions $u_l^{H,RB}$ and we want to approximate the boundary flux across $\partial\Omega$. The approximate flux can be constructed by assembling the function $\Lambda_{A_\sigma^{0,N}}^H g_l \in S^1(\partial\Omega, \mathcal{T}_H)$ such that

$$(40) \quad \int_{\partial\Omega} \Lambda_{A_\sigma^{0,N}}^H g_l v^H ds = B_{H,RB}(u_l^{H,RB}, v^H) \quad \forall v^H \in S_c^1(\Omega, \mathcal{T}_H),$$

where

$$B_{H,RB}(v^H, w^H) = \sum_{K \in \mathcal{T}_H} |K| A^{0,N}(\sigma(x_K)) \nabla v^H \cdot \nabla w^H.$$

Let us remark that $u_l^{H,RB}$ has been already computed, and so constructing $\Lambda_{A_\sigma^{0,N}}^H g_l$ leads to solving a linear systems whose unknowns are the values of the boundary flux at the nodes of $\partial\Omega$.

6.4. Convergence analysis. It is interesting to analyze how the numerical error intrinsic in the forward model affects the numerical posterior. To this end we will assume the forward model is approximated using the FE-HMM (no model order reduction). In this case the numerical flux is given by $\Lambda_{A_\sigma^{0,h}}^H g_l \in S^1(\partial\Omega, \mathcal{T}_H)$, where

$$(41) \quad \int_{\partial\Omega} \Lambda_{A_\sigma^{0,h}}^H g_l v^H \, ds = B_H(u_l^H, v^H) \quad \forall v^H \in S_c^1(\Omega, \mathcal{T}_H).$$

Hence, we define the operator $F^{H,h} : U \rightarrow \mathbb{R}^{JL}$, $F^{H,h}(\sigma) = \text{vec}(\{f_{jl}^{H,h}(\sigma)\}_{\substack{1 \leq j \leq J \\ 1 \leq l \leq L}}$,

$$(42) \quad f_{jl}^{H,h}(\sigma) = \left\langle \Lambda_{A_\sigma^h}^H g_l, \phi_j \right\rangle_{H^{-1/2}(\partial\Omega), H^{1/2}(\partial\Omega)}, \quad j = 1, \dots, J, l = 1, \dots, L,$$

and the corresponding potential function $\Phi^{H,h} : C^0(\bar{\Omega}) \times \mathbb{R}^{JL} \rightarrow \mathbb{R}$ given by

$$(43) \quad \Phi^{H,h}(\theta, z) = \frac{1}{2} \|z - G^{H,h}(\theta)\|_{C_e}^2,$$

where $G^{H,h} : F^{H,h} \circ P$, and P is one of the maps introduced in section 2.3. We denote as $\mu^{H,h}(\theta|z)$ the numerical posterior given by

$$(44) \quad \frac{d\mu^{H,h}(\theta|z)}{d\mu_{pr}(\theta)} \propto \exp(-\Phi^{H,h}(\theta, z)).$$

The following theorem establishes the convergence rate of the numerical posterior toward the true posterior $\mu^0(\theta|z)$ in the Hellinger metric. In particular, this convergence rate is the same as the rate of the discretization error of the forward model. Since convergence rates for the forward model are available only in the case where $\sigma \in W^{1,\infty}(\bar{\Omega})$, we assume in what follows that each draw from the prior μ_{pr} is in $W^{1,\infty}(\bar{\Omega})$ and that $P : \theta \mapsto \sigma$ is $P_1(\cdot) = \exp(\cdot)$.

Theorem 6. *Let μ^0 and $\mu^{H,h}$ be defined as in (13) and (44), respectively. Let the assumptions of Theorem 3 be satisfied together with (22). Assume that $A^0(P(\theta(\cdot))) \in W^{1,\infty}(\Omega, \text{Sym}_d)$ and that $P(\theta) = P_1(\theta) = \exp(\theta)$. Assume that $\mu_{pr}(W^{1,\infty}(\bar{\Omega})) = 1$ and that $u^0 \in H^2(\Omega)$ for each $l = 1, \dots, L$. Then we have that*

$$(45) \quad d_{Hell}(\mu^0, \mu^{H,h}) \leq C \left(H + \left(\frac{h}{\varepsilon} \right)^2 \right),$$

where C is a constant independent of H , h , and ε .

Proof. From the definition of the Hellinger distance we have

$$(46) \quad \begin{aligned} 2d_{Hell}^2(\mu^0, \mu^{H,h}) &= \int_{W^{1,\infty}(\bar{\Omega})} \left(\sqrt{\frac{d\mu^0}{d\mu_{pr}}} - \sqrt{\frac{d\mu^{H,h}}{d\mu_{pr}}} \right)^2 \mu_{pr}(d\theta) \\ &= \int_{W^{1,\infty}(\bar{\Omega})} \left(\frac{1}{\sqrt{K^0}} \exp\left(-\frac{1}{2}\Phi^0(\theta, z)\right) - \frac{1}{\sqrt{K^{H,h}}} \exp\left(-\frac{1}{2}\Phi^{H,h}(\theta, z)\right) \right)^2 \mu_{pr}(d\theta), \end{aligned}$$

where K^0 and $K^{H,h}$ are the two normalization constants such that $\mu^0(\theta|z)$ and $\mu^{H,h}(\theta|z)$ are probability measures, i.e.,

$$K^0 = \int_{W^{1,\infty}(\bar{\Omega})} \exp(-\Phi^0(\theta, z)) \mu_{pr}(d\theta), \quad K^{H,h} = \int_{W^{1,\infty}(\bar{\Omega})} \exp(-\Phi^{H,h}(\theta, z)) \mu_{pr}(d\theta).$$

By computations similar to the proof of Theorem 5 we obtain

$$\begin{aligned} 2d_{Hell}^2(\mu^0, \mu^{H,h}) &\leq C \int_{W^{1,\infty}(\bar{\Omega})} (\Phi^0(\theta, z) - \Phi^{H,h}(\theta, z))^2 \mu_{pr}(d\theta) \\ (47) \quad &\leq C \int_{W^{1,\infty}(\bar{\Omega})} (2\|z\|_{C_e} + \|G^0(\theta)\|_{C_e} + \|G^{H,h}(\theta)\|_{C_e})^2 \|G^0(\theta) - G^{H,h}(\theta)\|_{C_e}^2 \mu_{pr}(d\theta). \end{aligned}$$

We know that (see Theorem 3) if $P = P_1$ both $\|G^0(\theta)\|_{C_e}$ and $\|G^{H,h}(\theta)\|_{C_e}$ are bounded by some scalar multiple of $\beta_{\|\theta\|_{L^\infty(\Omega)}}^2 \alpha_{\|\theta\|_{L^\infty(\Omega)}}^{-1}$, which is square integrable with respect to μ_{pr} . Moreover, we also have that

$$\|G^0(\theta) - G^{H,h}(\theta)\|_{C_e} \leq C \sum_{j=1}^J \sum_{l=1}^L |\left\langle \left(\Lambda_{A_{P_1(\theta)}^0} - \Lambda_{A_{P_1(\theta)}^{0,h}}^H \right) g_l, \phi_j \right\rangle_{H^{-1/2}(\partial\Omega), H^{1/2}(\partial\Omega)}|.$$

Using integration by parts together with the Cauchy–Schwarz inequality we get

$$\|G^0(\theta) - G^{H,h}(\theta)\|_{C_e} \leq C \sup_l \left\| A^0(P_1(\theta)) \nabla u^0 - A^{0,h}(P_1(\theta)) \nabla u^H \right\|_{L^2(\Omega)} \sup_j \|\nabla \tilde{\phi}_j\|_{L^2(\Omega)},$$

where $\tilde{\phi}_j$ is a function in $H^1(\Omega)$ whose trace is ϕ_j . Using standard FE-HMM a priori error estimates (see [1], for example) we obtain

$$(48) \quad \|G^0(\theta) - G^{H,h}(\theta)\|_{C_e} \leq C \left(H + \left(\frac{h}{\varepsilon} \right)^2 \right),$$

where C is independent of H , h , and ε . Hence, using (47) and (48) together with the Lebesgue’s dominated convergence theorem the result follows. ■

In [4] faster order convergence for the flux at the boundary was established under additional regularity assumptions. Such a result allows us to state the following corollary.

Corollary 1. *Let $A^0(P(\theta(\cdot))) \in W^{2,\infty}(\Omega, Sym_d)$, $P(\theta) = P_1(\theta) = \exp(\theta)$, $\mu_{pr}(W^{2,\infty}(\bar{\Omega})) = 1$, and $u^0 \in H^3(\Omega)$ for each $l = 1, \dots, L$. Then, we can establish a faster convergence rate for the Hellinger distance by using the error estimate for the $L^2(\partial\Omega)$ -norm of the boundary flux obtained in [4], namely*

$$(49) \quad d_{Hell}(\mu^0, \mu^{H,h}) \leq C \left(H^{3/2} + \left(\frac{h}{\varepsilon} \right)^{3/2} \right).$$

Remark 4. Let us note that for a given accuracy, the computational cost for solving the micro problems is independent of ε , since the size of the micro domain $\delta \geq \varepsilon$ is proportional

to ε . Let N_{mac} and N_{mic} be the degrees of freedom in one direction for the macro domain and the micro domain, respectively. Then (45) can be rewritten as

$$d_{Hell} \left(\mu^0, \mu^{H,h} \right) \leq C \left(N_{mac}^{-1} + N_{mic}^{-2} \right).$$

Hence, by choosing $N_{mac} = N_{mic}^2 = N$ for optimal convergence, the total complexity is $\mathcal{O}(N^{2d})$ for an accuracy of $\mathcal{O}(N^{-1})$. Finally, we emphasize that the estimates (45) and (49) are valid under the assumptions that the multiscale tensor is locally periodic, the slow variable of the tensor is collocated at the macro quadrature points, and periodic boundary conditions are set for solving the micro problems. If such assumptions are not satisfied, e.g., in the case of homogenization in random media, an additional modeling error has to be taken into account, which vanishes as $\varepsilon \rightarrow 0$ (for fixed sampling domain size δ) or, equivalently, as $\delta \rightarrow \infty$ (for fixed ε). This study has been addressed in [5].

Remark 5. If the forward model is approximated by the RB-FE-HMM, the error due to the micro discretization is usually negligible as the reduced space is built with precomputed micro functions computed on a very fine discretization. However, a new error enters into the estimate, namely the error due to the model order reduction. This error is based on the distance between the reduced space $S^N(Y)$ and $S^1(Y, \mathcal{T}_h)$. Such distance can be quantified by means of the notion of Kolmogorov N -width (see [3], for example).

6.5. Summary of the numerical procedure to solve the multiscale inverse problem. We denote as \mathcal{T}_H the macro triangulation and as N_H the number of macro DOFs. In the discrete setting, the prior measure $\mu_{pr} = \mathcal{N}(\theta_{pr}, C_{pr})$ is replaced by $\mathcal{N}(\theta_{pr}^H, C_{pr}^H)$, where $\theta_{pr}^H = \mathcal{I}^H \theta_{pr}$, \mathcal{I}^H is the linear interpolation operator, and $C_{pr}^H \in \mathbb{R}^{N_H \times N_H}$ is a symmetric positive matrix which approximates the covariance operator C_{pr} . We denote as $\{\varphi_k^H, \lambda_k^H\}_{k=1}^{N_H}$ the orthonormal set of eigenvectors and eigenvalues of C_{pr}^H . Each $\theta^H \sim \mathcal{N}(\theta_{pr}^H, C_{pr}^H)$ can then be represented as

$$\theta^H(x) = \theta_{pr}^H(x) + \sum_{k=1}^{N_H} \sqrt{\lambda_k^H} \eta_k \varphi_k^H(x),$$

where $\{\eta_k\}_{k=1}^{N_H}$ is an i.i.d. sequence with $\eta_1 \sim \mathcal{N}(0, 1)$. If we truncate the Karhunen–Loëve expansion at the K largest eigenvalues we obtain

$$\theta^{H,K}(x) = \theta_{pr}^H(x) + \sum_{k=1}^K \sqrt{\lambda_k^H} \eta_k \varphi_k^H(x).$$

In what follows we will use the notation $\theta_{\boldsymbol{\eta}}^{H,K}$ to emphasize the dependence on $\boldsymbol{\eta} = (\eta_1, \dots, \eta_K)^\top$. The numerical scheme for solving the multiscale inverse problem, given the perturbed observations $z \in \mathbb{R}^{JL}$, can then be summarized as follows:

1. Compute in an offline stage a reduced space of precomputed microscopic functions as described in section 6.
2. Compute in an offline stage the set $\{\varphi_k^H, \lambda_k^H\}_{k=1}^K$ of eigenfunctions and eigenvalues of the prior covariance C_{pr}^H , so that for a point $\boldsymbol{\eta} \in \mathbb{R}^K$ we have that

$$\theta_{\boldsymbol{\eta}}^{H,K}(x) = \theta_{pr}^H(x) + \sum_{k=1}^K \sqrt{\lambda_k^H} \eta_k \varphi_k^H(x).$$

3. Sample online from the posterior distribution. In particular, for a new realization $\boldsymbol{\eta}$, in order to evaluate $\pi^0(\boldsymbol{\eta}|z)$, do the following for each $l = 1, \dots, L$:
 - Solve (38) for $\sigma = P(\theta_{\boldsymbol{\eta}}^{H,K})$.
 - Approximate the corresponding flux at the boundary by solving (40) and evaluate (11).

7. Numerical experiments. In this section we will present some numerical experiments to illustrate our multiscale Bayesian algorithm for inverse problems. We start by explaining how observed data are collected. We then solve the inverse problem for different macroscopic parametrizations. At first, we consider an affine parametrization of the form $A^\varepsilon(x) = \sigma^*(x)B^\varepsilon(x) = \sigma^*(x)B(x/\varepsilon)$, so that the function σ^* controls the amplitude of the characteristic micro oscillations. Let us point out that, for this choice, we have that $A^0(x) = \sigma^*(x)B^0$, and thus the use of reduced basis methods for solving the forward problem is not required. This simple problem allows us to perform numerous tests to quantify the sensitivity of the method with respect to the several parameters involved in the approximation, such as ε , the size of the microscopic oscillations, K , the number of terms in the truncated Karhunen–Loèvre expansion, and L , the number of Dirichlet data. Then, we will consider two different non-affine macroscopic parametrizations, one controlling the orientation of the micro oscillations, the other the volume fraction of a hypothetical layered material. For these problems, we make the following choice of parameters for the RB-FE-HMM offline stage: $h/\varepsilon = 1/64$, $\delta = \varepsilon$, $tol_{RB} = 10^{-11}$, where tol_{RB} is a prescribed tolerance used as the stopping criterion for the greedy algorithm employed to select the reduced basis functions.

7.1. Setup. The computational domain is the unit square

$$\Omega = \{x = (x_1, x_2) : 0 < x_1, x_2 < 1\}.$$

We approximate the solution to problem (1) by means of the FEM using a very fine discretization $h_{obs} \ll \varepsilon$. The forward homogenized problem is instead computed using a macro mesh size $H = 1/64$. The problem is solved for different Dirichlet conditions $\{g_l\}_{l=1}^L$. In particular we take $\{g_l\}_{l=1}^L = \{\sqrt{\lambda_l}\varphi_l\}_{l=1}^L$, where $\{(\lambda_l, \varphi_l)\}_{l=1}^L$ are the L eigenpairs corresponding to the L smallest eigenvalues associated to the one-dimensional discrete Laplacian operator. Each g_l is then projected on the boundary $\partial\Omega$ to define the corresponding Dirichlet condition. This procedure ensures that the functions $\{g_l\}_{l=1}^L$ are smooth and orthonormal, so that each experiment contributes differently one from another. Moreover $\|\nabla g_l\|_{L^2(\partial\Omega)} < C$, where C is a constant independent of L . Finally, we consider $J = 12$ boundary portions $\Gamma_j \subset \partial\Omega$, three for each side of the computational domain as shown in Figure 1. Each Γ_j has length equal

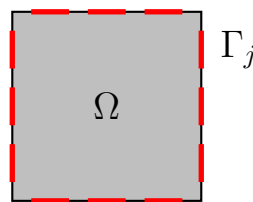


Figure 1. Picture representing the computational domain Ω and the boundary portions Γ_j used to compute the observations.

to 0.2. The functions ϕ_j appearing in (5) are hat functions with $\text{supp}(\phi_j) = \Gamma_j$ and which take value one at the midpoint of each Γ_j . Once the observed data have been computed, they are perturbed by the noise given by $e = 10^{-4}w$, $w \sim \mathcal{N}(0, I)$. Let p_i and p_j be two nodes of the macro triangulation \mathcal{T}_H , and let N_H the total number of nodes defining \mathcal{T}_H . Note that $N_H = H^{-2}$. The covariance matrix in the prior measure $\mu_{pr} = \mathcal{N}(\theta_{pr}^H, C_{pr}^H)$ is then $C_{pr}^H \in \mathbb{R}^{N_H \times N_H}$ defined as

$$(50) \quad (C_{pr}^H)_{ij} = \gamma \exp\left(-\frac{\|p_i - p_j\|_2}{\lambda}\right), \quad \gamma, \lambda \in \mathbb{R}^+,$$

while the prior mean is $\theta_{pr}^H = \mathcal{I}^H \theta_{pr}$, where θ_{pr} is some function in $C^0(\overline{\Omega})$. We set different values for γ , λ , and θ_{pr} , depending on the macroscopic parametrization we want to retrieve. In particular, $\lambda > 0$ is a correlation length that describes how the values at different positions of the functions supported by the prior measure are related, while $\gamma > 0$ is the amplitude scaling factor. Let us point out that the covariance matrix C_{pr}^H belongs to the family of Matérn covariances. In particular, we have that each draw from $\mathcal{N}(\theta_{pr}^H, C_{pr}^H)$ with C_{pr}^H defined as in (50) is a.s. s -Hölder continuous with $0 < s < 1/2$ for θ_{pr}^H sufficiently regular (see [21] for more details).

7.2. Two-dimensional affine parametrization (amplitude of oscillations). In this first set of numerical experiments we consider the tensor $A_{\sigma^*}^\varepsilon$ given by

$$\begin{aligned} A_{11}(\sigma^*(x), x/\varepsilon) &= \sigma^*(x) \left(\cos^2\left(\frac{2\pi x_1}{\varepsilon}\right) + 1 \right), \\ A_{22}(\sigma^*(x), x/\varepsilon) &= \sigma^*(x) \left(\sin\left(\frac{2\pi x_2}{\varepsilon}\right) + 2 \right), \\ A_{12}(\sigma^*(x), x/\varepsilon) &= A_{21}(\sigma^*(x), x/\varepsilon) = 0, \end{aligned}$$

where

$$\sigma^*(x) = 1.3 + 0.3\mathbb{1}_{D_1} - 0.4\mathbb{1}_{D_2},$$

and

$$\begin{aligned} D_1 &= \{x = (x_1, x_2) : (x_1 - 5/16)^2 + (x_2 - 11/16)^2 \leq 0.025\}, \\ D_2 &= \{x = (x_1, x_2) : (x_1 - 11/16)^2 + (x_2 - 5/16)^2 \leq 0.025\}. \end{aligned}$$

The task of the problem is to retrieve the function σ^* , which is shown together with the component A_{11}^ε of the tensor, $\varepsilon = 1/64$, in Figure 2.

Sensitivity with respect to ε . We start by studying how different choices of ε can affect our predictions. The computations are reported later in Figure 4. We briefly describe the setting. We compute numerically by means of a resolved FEM synthetic observations for different values of $\varepsilon = \{1/4, 1/8, 1/16, 1/8, 1/64\}$, for $L = 6$ different Dirichlet conditions. We consider a truncated Karhunen–Loëve expansion with $K = 60$. A priori, we only assume σ^* to be positive, hence we consider a lognormal prior for this first set of numerical tests.

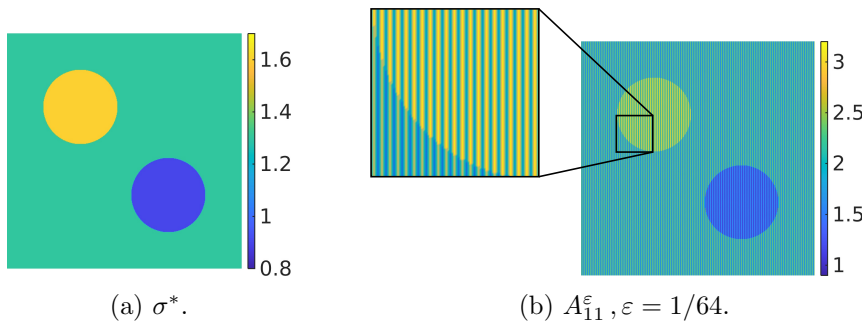


Figure 2. Representation of the true spatial field σ^* and the first component of the highly oscillating tensor for the problem considered in section 7.2.

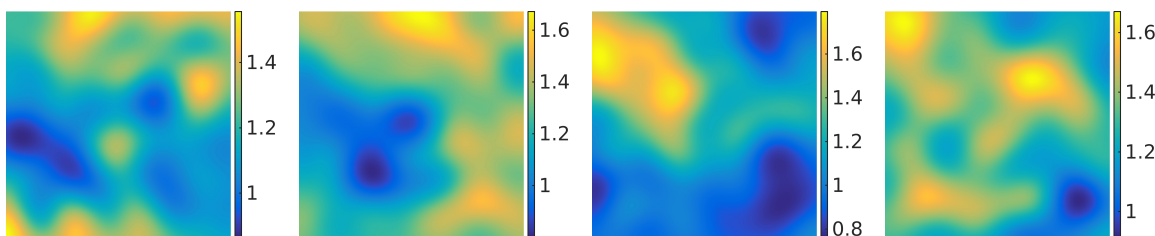


Figure 3. Four samples from the prior density used in the problem considered in section 7.2.

We remark that the condition (22) holds for the parameterized tensor considered in this first set of numerical experiments. Indeed we have that $A(\sigma(x), x/\varepsilon)$ is of the form $\sigma(x)B(x/\varepsilon)$, and hence $\alpha_{\|\theta\|_{L^\infty(\Omega)}}^{-1} \beta_{\|\theta\|_{L^\infty(\Omega)}}^2 \leq C \exp(3\|\theta\|_{L^\infty(\Omega)})$ which is square integrable with respect to the Gaussian measure on $C^0(\overline{\Omega})$. The prior measure μ_{pr} on $\theta \in C^0(\overline{\Omega})$ is $\mathcal{N}(\theta_{pr}^H, C_{pr}^H)$, with $\theta_{pr} = \log 1.3$ and C_{pr}^H defined in (50) with $\gamma = 0.05$ and $\lambda = 0.5$. In particular the choice of $\theta_{pr} = \log 1.3$ is such that the resulting lognormal distribution on the admissible set U has median 1.3. We then push each draw θ into the admissible set through the function $P_1 : \theta \mapsto \exp(\theta)$. Examples of realizations from the lognormal prior are shown in Figure 3. We draw then 2×10^5 samples from the posterior distribution (30) using the MH algorithm. The parameter s is set to 0.01. The starting point is $\boldsymbol{\eta}^1 = 0 \in \mathbb{R}^K$. With this choice of the parameters we obtain an acceptance rate of about 27% for all choices of ε . In Figure 4 we plot for each ε the quantities $P_1(\mathbb{E}[\theta^{H,K}])$, $\mathbb{E}[P_1(\theta^{H,K})]$, and the variance $\text{Var}[P_1(\theta^{H,K})]$, where \mathbb{E} denotes the approximated expectation obtained from the MH algorithm. The first quantity is produced by computing first the mean on the Banach space $C^0(\overline{\Omega})$ and then pushing it into the admissible set U through $P_1 : C^0(\overline{\Omega}) \rightarrow U$. Moreover, we also show the approximation of the posterior density for the first three coefficients in the truncated Karhunen–Loëve expansion. We can observe that as ε gets smaller, these densities stabilize and converge to the same posterior. We notice that with $\varepsilon = 1/4$ we get inaccurate predictions about the quantity of interest, while already with $\varepsilon = 1/8$ the approximation of the posterior mean is in good agreement with Figure 2. The source of error for large ε comes from the discrepancy between the multiscale model from where the observations are obtained and the homogenized model used for solving the inverse problem.

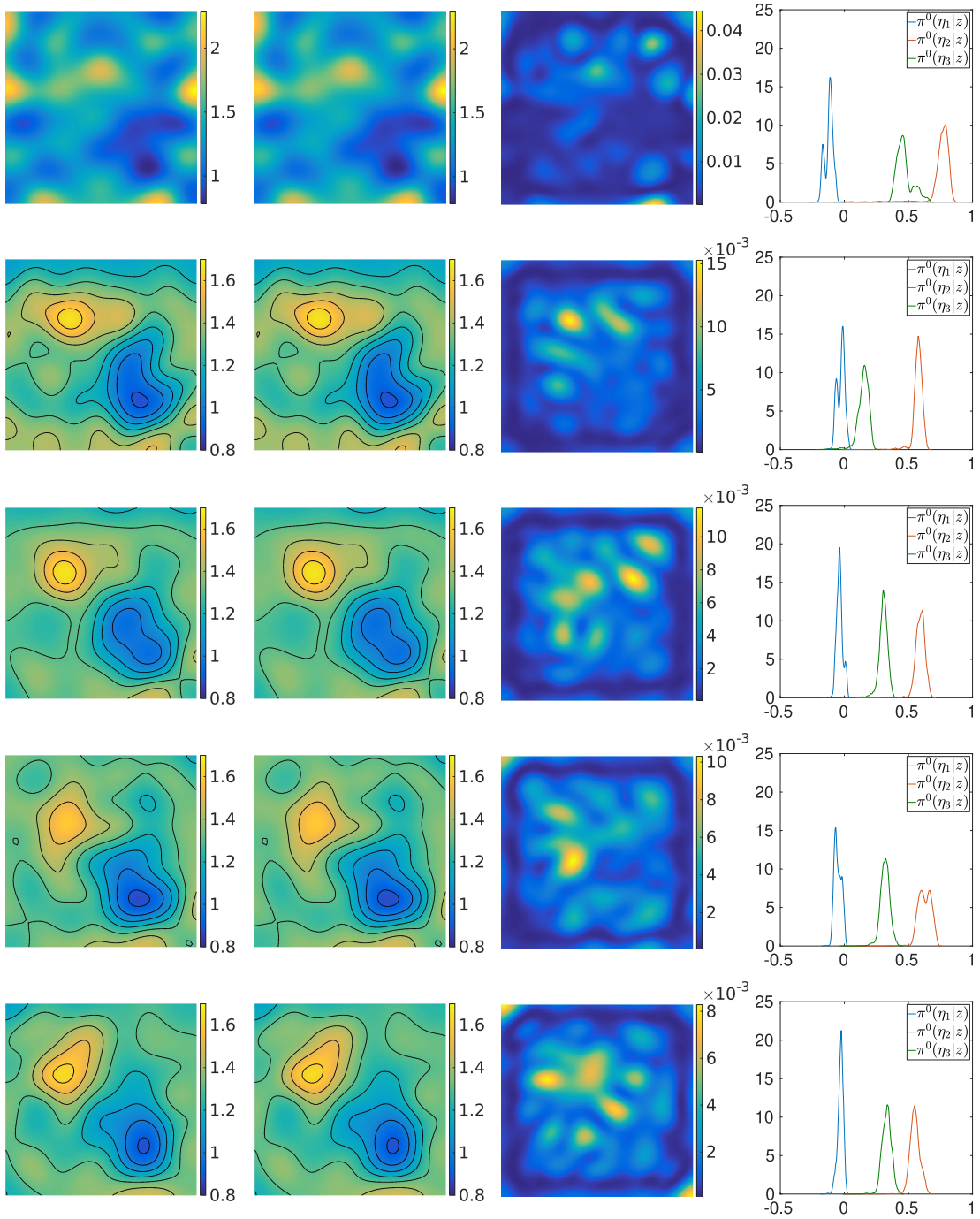


Figure 4. Comparison of numerical approximations of the posterior density for the problem considered in section 7.2, obtained with different values of ϵ . From left to right the plotted quantities are $P_1(\mathbb{E}[\theta^{H,K}])$, $\mathbb{E}[P_1(\theta^{H,K})]$, $\text{Var}[P_1(\theta^{H,K})]$, and the posterior density of the three first coefficients of the truncated Karhunen–Loeve expansion, corresponding to $\epsilon = \{1/4, 1/8, 1/16, 1/32, 1/64\}$. The length scale ϵ decreases from the top to the bottom. The other parameters are $H = 1/64$, $L = 6$, $K = 60$.

Approximation of the homogenization error distribution. As seen in Figure 4, for large values of ε the homogenization error (the discrepancy between the fine scale and the homogenized problems) pollutes the posterior prediction. Therefore, we perform again the same experiment for $\varepsilon = 1/4$, but taking into account the homogenization error as described in section 4.2. We approximate the homogenization error distribution by computing its mean and covariance using Algorithm 1, and we include these quantities in the posterior density definition according to (28). We perform the experiment for various numbers of sample sizes M to approximate the homogenization error distribution, namely $M = \{5, 10, 20\}$. The parameters such as K and L are identical to the previous numerical test. Numerical results are shown in Figure 5. In particular we can observe how already with $M = 5$ we can manage to significantly improve the results reported in Figure 4 for $\varepsilon = 1/4$.

Sensitivity with respect to L (number of Dirichlet data). Next, we investigate the sensitivity of the approximated solution with respect to the parameter L , denoting the number

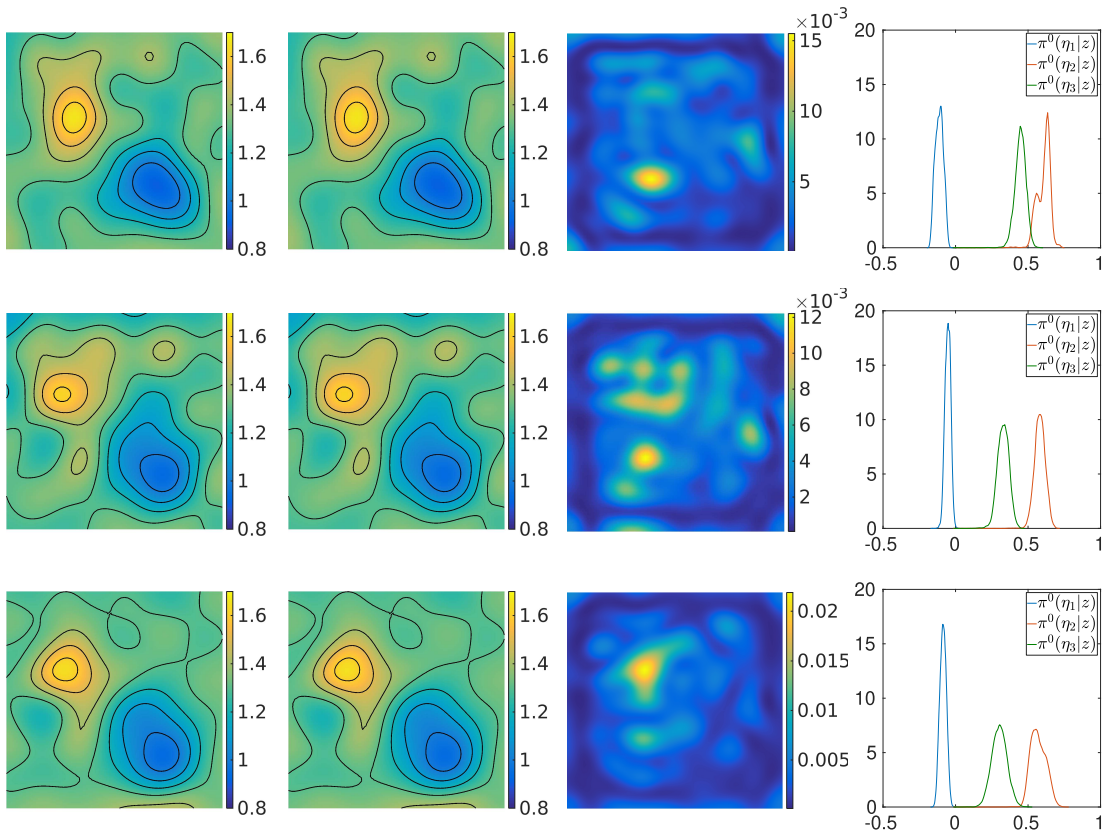


Figure 5. Comparison of numerical approximations of the posterior density for the problem considered in section 7.2 obtained with $\varepsilon = 1/4$, for different values of M , the sample size used to approximate the homogenization error distribution. From left to right the plotted quantities are $P_1(\mathbb{E}[\theta^{H,K}])$, $\mathbb{E}[P_1(\theta^{H,K})]$, $\text{Var}[P_1(\theta^{H,K})]$, and the posterior density of the three first coefficients of the truncated Karhunen–Loeve expansion. The value of M is 5 in the first row, 10 in the second row, and 20 in the third row. The other parameters are $H = 1/64$, $L = 6$, $K = 60$.

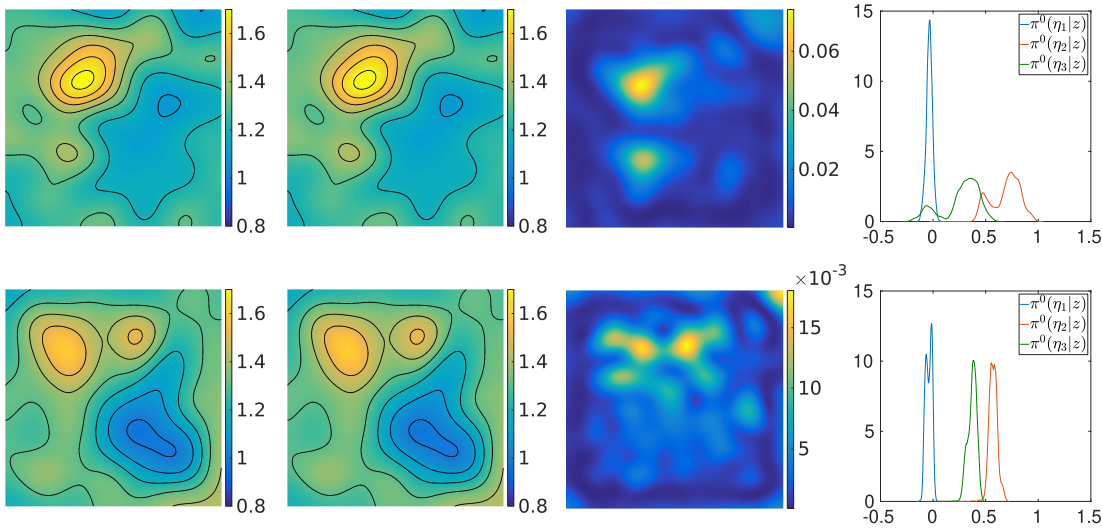


Figure 6. Comparison of numerical approximations of the posterior density for the problem considered in section 7.2 obtained for different values of L , the number of Dirichlet data. From left to right the plotted quantities are $P_1(\mathbb{E}[\theta^{H,K}])$, $\mathbb{E}[P_1(\theta^{H,K})]$, $\text{Var}[P_1(\theta^{H,K})]$, and the posterior density of the three first coefficients of the truncated Karhunen–Loève expansion. In the first row $L = 2$, in the second one $L = 4$. For $L = 6$ see the last row in Figure 4. The other parameters are $H = 1/64$, $\varepsilon = 1/64$, $K = 60$.

of different Dirichlet conditions used to produce the observations. The setting is the same as in the previous numerical experiments, except that ε is fixed and equal to $1/64$, while $L = \{2, 4, 6\}$. Numerical results are shown in Figure 6. We notice that for $L = 2$ the variance is significantly larger than for $L = 4$ or $L = 6$, which indicates more uncertainty about the approximated solution. This is also visible from the approximation of the posterior density obtained for the three first coefficients of the Karhunen–Loève expansion.

Sensitivity with respect to K (number of terms in the truncated Karhunen–Loève expansion). Finally, we examine how the size of the truncated Karhunen–Loève expansion affects our predictions. We perform experiments for $K = \{10, 20, 30, 40, 50, 60\}$, while L and ε are fixed, set to 6 and $1/64$, respectively. The results shown in Figure 7 illustrate that by increasing the number of eigenvalues/eigenfunctions, we obtain a better sampling of the quantity of interest.

7.3. Two-dimensional nonaffine parametrization (orientation of oscillations). Now we consider the case where the function σ^* controls the angle of the oscillations which characterize the full tensor $A_{\sigma^*}^\varepsilon$. The tensor is defined as

$$(51) \quad \begin{aligned} A_{11}(\sigma^*(x), x/\varepsilon) &= \sin\left(\frac{4\pi\mathbf{e}^{1^\top} Qx}{\varepsilon}\right) + 1.5, \\ A_{22}(\sigma^*(x), x/\varepsilon) &= \cos^2\left(\frac{2\pi\mathbf{e}^{2^\top} Qx}{\varepsilon}\right) + 1, \\ A_{12}(\sigma^*(x), x/\varepsilon) &= A_{21}(\sigma^*(x), x/\varepsilon) = 0, \end{aligned}$$

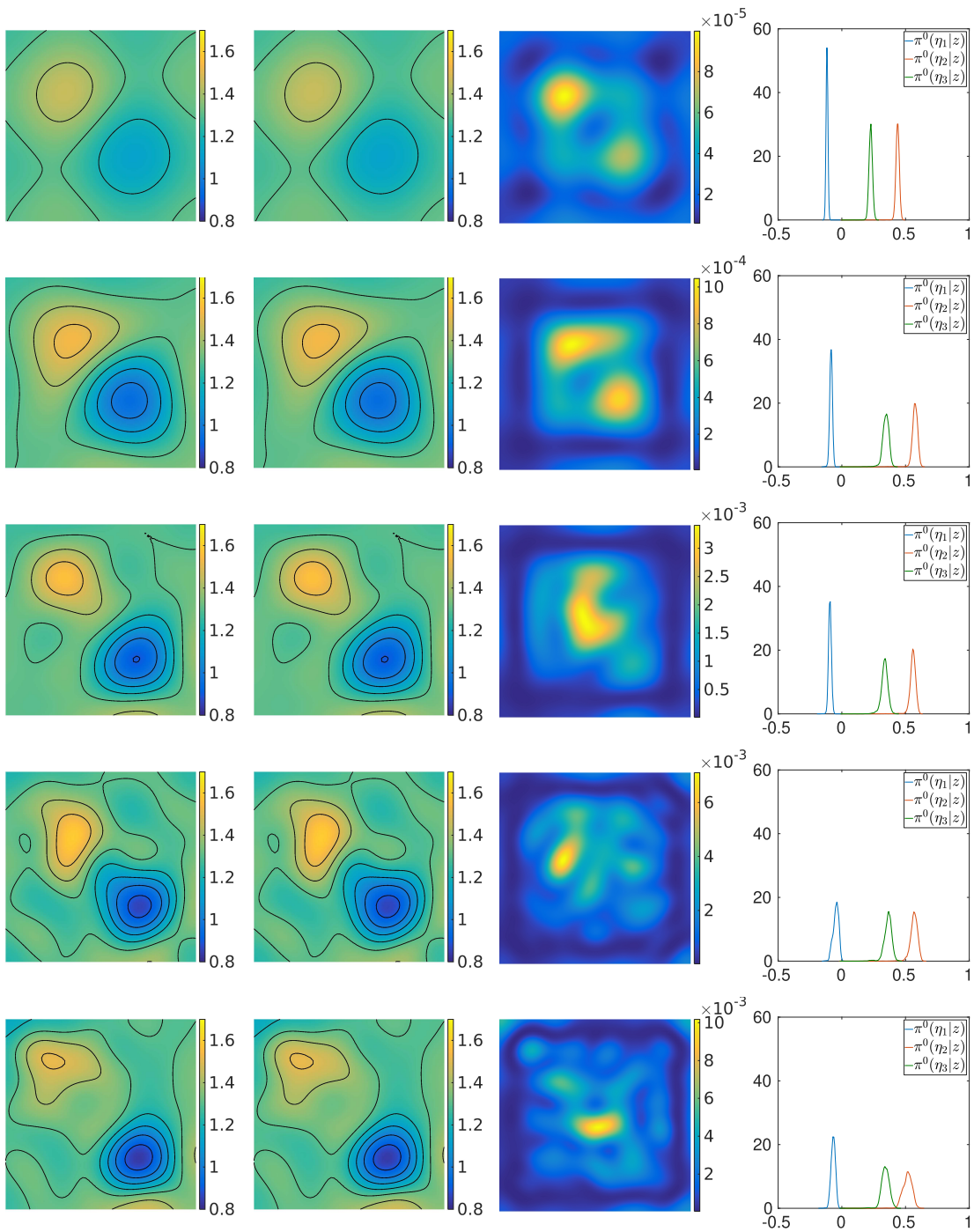


Figure 7. Comparison of numerical approximations of the posterior density for the problem considered in section 7.2 obtained for different values of K , the number of coefficients in the truncated Karhunen–Loève expansion. From left to right the plotted quantities are $P_1(\mathbb{E}[\theta^{H,K}])$, $\mathbb{E}[P_1(\theta^{H,K})]$, $\text{Var}[P_1(\theta^{H,K})]$, and the posterior density of the three first coefficients of the truncated Karhunen–Loève expansion, corresponding to $K = \{10, 20, 30, 40, 50\}$. The parameter K increases from the top to the bottom. For $K = 60$ see the last row in Figure 4. The other parameters are $H = 1/64$, $\varepsilon = 1/64$, $L = 6$.

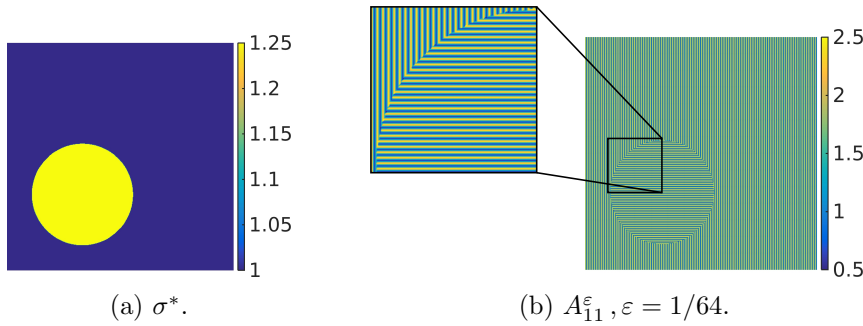


Figure 8. Representation of the true spatial field σ^* and the first component of the highly oscillating tensor for the nonaffine case considered in section 7.3 (orientation of oscillations).

where $Q = Q(\sigma^*(x))$ is a rotation matrix depending on $\sigma^* : \Omega \rightarrow \mathbb{R}$,

$$(52) \quad Q(\sigma^*(x)) = \begin{pmatrix} \cos(2\pi\sigma^*(x)) & \sin(2\pi\sigma^*(x)) \\ -\sin(2\pi\sigma^*(x)) & \cos(2\pi\sigma^*(x)) \end{pmatrix},$$

and

$$\sigma^*(x) = a + b\mathbb{1}_D, \quad D \subset \Omega, a, b \in \mathbb{R}.$$

We consider the case where D is the circle defined as

$$D = \{x = (x_1, x_2) : (x_1 - 1/3)^2 + (x_2 - 1/3)^2 \leq 0.05\}.$$

In Figure 8 we show the function σ^* and the first component of the tensor A_{11}^ε . From (51) and (52) it can be observed that different values of a and b for σ^* can lead to the same rotation of the oscillations, and in general to the same tensor $A_{\sigma^*}^\varepsilon$. To ensure uniqueness we assume to know a priori the values of a and b . We take $a = 1$ and $b = 0.25$. Our task is thus to recover the region $D \subset \Omega$. To do so, we consider a level set prior for the unknown, defined using the function $P_2 : C^0(\bar{\Omega}) \rightarrow U$ introduced in section 2.3. The prior measure on $C^0(\bar{\Omega})$ is defined as in (50) with $\theta_{pr} = 1$, $\gamma = 0.025$, and $\lambda = 0.5$. Hence, we apply the map P_2 to each draw from μ_{pr} to obtain a level set sample, i.e.,

$$P_2(\theta) = 1\mathbb{1}_{\Omega_1} + 1.25\mathbb{1}_{\Omega_2},$$

where

$$\Omega_1 = \{x \in \Omega : -\infty < \theta(x) \leq 1\}, \quad \Omega_2 = \{x \in \Omega : 1 < \theta(x) < \infty\},$$

so that $\bar{\Omega} = \Omega_1 \cup \Omega_2$, $\Omega_1 \cap \Omega_2 = \emptyset$. Four examples of draws from the level set prior are reported in Figure 9.

We obtain data for $\varepsilon = 1/64$ and we approximate the homogenization error distribution by using Algorithm 1 with $M = 20$. The parameters K and L are set to 60 and 6, respectively. Then, we approximate the posterior by using the MH algorithm by drawing 4×10^5 samples using $s = 0.02$. For this choice of the parameters, we get an acceptance ratio during the sampling of about 73%. In Figure 10 we plot the quantities $P_2(\mathbb{E}[\theta^{H,K}])$, $\mathbb{E}[P_2(\theta^{H,K})]$, and $\text{Var}[P_2(\theta^{H,K})]$. In particular $P_2(\mathbb{E}[\theta^{H,K}])$ preserves the binary field property of the admissible set, while the estimate $\mathbb{E}[P_2(\theta^{H,K})]$ gives a better understanding of the uncertainty across the

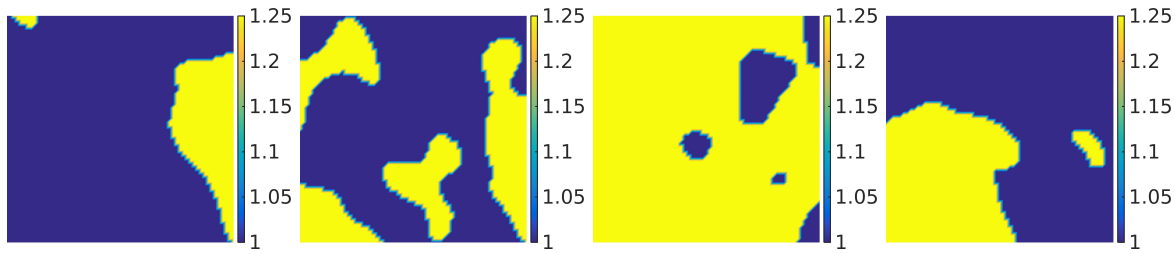


Figure 9. Four samples from the level set prior used in the problem considered in section 7.3.

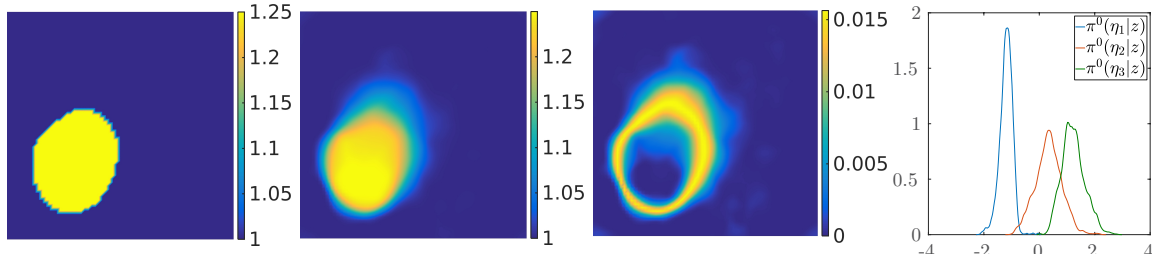


Figure 10. Numerical results for the nonaffine parametrization considered in section 7.3 (orientation of oscillations). From left to right the plotted quantities are $P_2(\mathbb{E}[\theta^{H,K}])$, $\mathbb{E}[P_2(\theta^{H,K})]$, $\text{Var}[P_2(\theta^{H,K})]$, and the posterior density of the three first coefficients of the truncated Karhunen–Loëve expansion. The values of the parameters are $H = 1/64$, $\varepsilon = 1/64$, $M = 20$, $L = 6$, $K = 60$.

interface where the discontinuity takes place. This uncertainty is also reflected by the plot of the variance $\text{Var}[P_2(\theta^{H,K})]$. The numerical results show good agreement with Figure 8.

7.4. Two-dimensional nonaffine parametrization (volume fraction). We conclude the numerical experiments by considering the case where $A_{\sigma^*}^\varepsilon$ represents the conductivity of a hypothetical two-phase layered material. In this case the macroscopic function $\sigma^* : \Omega \rightarrow [0, 1]$ determines the volume fraction of each component. Then tensor is defined as

$$(53) \quad A_{11}(\sigma^*(x), x/\varepsilon) = A_{22}(\sigma^*(x), x/\varepsilon) = \begin{cases} 2 & \text{if } 0 \leq (x_2 \bmod \varepsilon)/\varepsilon < \sigma^*(x), \\ 1 & \text{if } \sigma^*(x) \leq (x_2 \bmod \varepsilon)/\varepsilon < 1, \end{cases}$$

$$A_{12}(\sigma^*(x), x/\varepsilon) = A_{21}(\sigma^*(x), x/\varepsilon) = 0.$$

We consider the case where σ^* is defined as

$$\sigma^*(x) = \sum_{i=1}^n c_i \mathbb{1}_{D_i}, \quad D_i \subset \Omega, c_i \in [0, 1],$$

$D_i \cap D_j = \emptyset$ for $i \neq j$, $\cup_{i=1}^n D_i = \Omega$. Again, we assume to know a priori the values $\{c_i\}_{i=1}^n$ that the function σ^* can take, and our goal is to recover the different regions $\{D_i\}_{i=1}^n$. We note that knowing the range of possible values for σ^* allows us to efficiently use the reduced basis method and in particular the EIM algorithm. For our problem we set $n = 4$, $c_1 = 0.8$, $c_2 = 0.6$, $c_3 = 0.4$, $c_4 = 0.2$, and we make the following choice for the sets $\{D_i\}_{i=1}^4$:

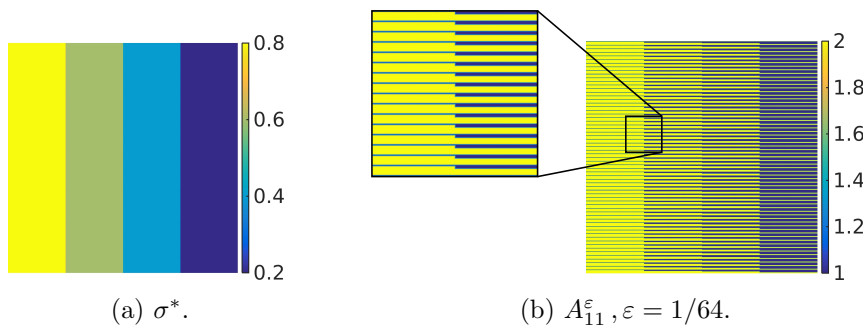


Figure 11. Representation of the true spatial field σ^* and the first component of the highly oscillating tensor for the nonaffine case considered in section 7.4 (volume fraction).

$$\begin{aligned}D_1 &= \{x = (x_1, x_2) : 0 \leq x_1 \leq 0.25\}, \\D_2 &= \{x = (x_1, x_2) : 0.25 < x_1 \leq 0.5\}, \\D_3 &= \{x = (x_1, x_2) : 0.5 < x_1 \leq 0.75\}, \\D_4 &= \{x = (x_1, x_2) : 0.75 < x_1 \leq 1\}.\end{aligned}$$

The true field σ^* and the first component of the multiscale tensor are shown in Figure 11.

We consider for this last numerical experiment a macro discretization with mesh size $H = 1/32$, and a level set prior. The Gaussian prior measure μ_{pr} on $C^0(\bar{\Omega})$ is the same used in the previous numerical tests, with $\theta_{pr} = 0.5$, $\gamma = 0.05$, $\lambda = 0.5$. The function $P_2 : C^0(\bar{\Omega}) \rightarrow U$ is instead defined as

$$P_2(\theta) = c_1 \mathbb{1}_{\Omega_1} + c_2 \mathbb{1}_{\Omega_2} + c_3 \mathbb{1}_{\Omega_3} + c_4 \mathbb{1}_{\Omega_4},$$

where

$$\begin{aligned}\Omega_1 &= \{x \in \Omega : 0.6 < \theta(x) < \infty\} , \\ \Omega_2 &= \{x \in \Omega : 0.4 < \theta(x) \leq 0.6\} , \\ \Omega_3 &= \{x \in \Omega : 0.2 < \theta(x) \leq 0.4\} , \\ \Omega_4 &= \{x \in \Omega : -\infty < \theta(x) \leq 0.2\} .\end{aligned}$$

Four samples from the considered level set prior are shown in Figure 12.

To solve the problem the observations are obtained for $\varepsilon = 1/64$. Nonetheless, we approximate offline the homogenization error distribution by using Algorithm 1 with $M = 20$. For the choice $\varepsilon = 1/64$, which is relatively small, this procedure might not be necessary since the homogenization error is expected to be small. However, since computing the homogenization error distribution is not particularly expensive in this case, we decide to include it in the solution of the inverse problem to allow for the most accurate numerical results. The parameters K and L are set to 60 and 6, respectively. We draw 4×10^5 samples from the posterior distribution using Algorithm 2 setting $s = 0.01$, leading to an acceptance ratio of 44%. The numerical results are shown in Figure 13 and are in good agreement with Figure 11.

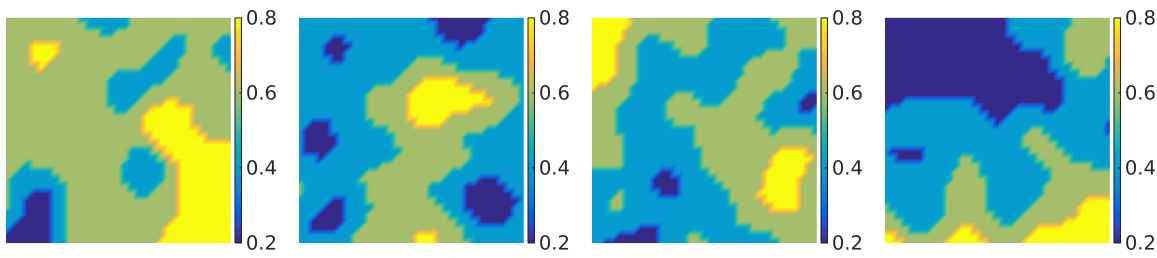


Figure 12. Four samples from the level set prior used in the problem considered in section 7.4.

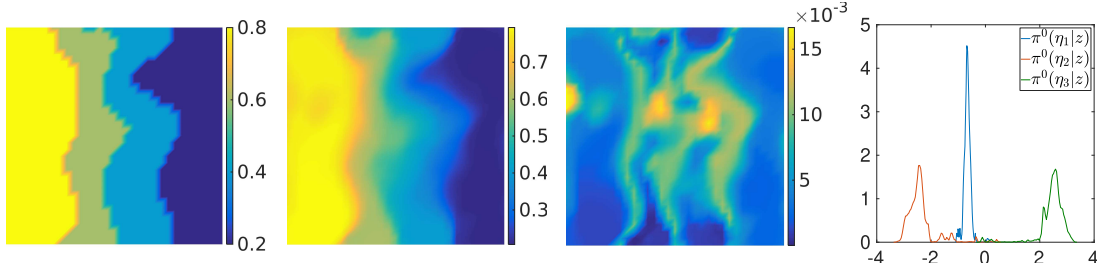


Figure 13. Numerical results for the nonaffine parametrization considered in section 7.4 (volume fraction). From left to right the plotted quantities are $P_2(\mathbb{E}[\theta^{H,K}])$, $\mathbb{E}[P_2(\theta^{H,K})]$, $\text{Var}[P_2(\theta^{H,K})]$, and the posterior density of the three first coefficients of the truncated Karhunen-Loeve expansion. $H = 1/32$, $\varepsilon = 1/64$, $M = 20$, $L = 6$, $K = 60$.

Conclusion. We have presented a new strategy for solving Bayesian multiscale inverse problems based on numerical homogenization and model order reduction. Our method allows us to recover the full fine scale tensor under the assumption that the microscopic structure of the fine scale tensor is known to us but its macroscopic behavior is unknown. Practical examples include multiphase mediums, whose constituents are known, but their respective volume fraction or macroscopic orientation are unknown. We then proved the existence and well-posedness of the effective posterior measure obtained by homogenization of the forward operator. By means of G-convergence we showed that the fine scale posterior measure converges to the homogenized posterior measure. At fixed size of the micro structure, we discussed a procedure to account for the homogenization error. We also proposed an efficient algorithm to sample from the posterior measure combining numerical homogenization and reduced basis techniques. Several numerical examples illustrating the efficiency of the proposed method and confirming our theoretical findings were also given.

REFERENCES

- [1] A. ABDULLE, *On a priori error analysis of fully discrete heterogeneous multiscale FEM*, Multiscale Model. Simul., 4 (2005), pp. 447–459.
- [2] A. ABDULLE, *The finite element heterogeneous multiscale method: A computational strategy for multiscale PDEs*, in Multiple Scales Problems in Biomathematics, Mechanics, Physics and Numerics, GAKUTO Internat. Ser. Math. Sci. Appl. 31, Gakkōtoshō, Tokyo, 2009, pp. 133–181.

- [3] A. ABDULLE AND Y. BAI, *Reduced basis finite element heterogeneous multiscale method for high-order discretizations of elliptic homogenization problems*, J. Comput. Phys., 231 (2012), pp. 7014–7036.
- [4] A. ABDULLE AND A. DI BLASIO, *Numerical homogenization and model order reduction for multiscale inverse problems*, Multiscale Model. Simul., 17 (2019), pp. 399–433.
- [5] A. ABDULLE AND A. DI BLASIO, *Bayesian numerical homogenization and probabilistic methods for inverse problems in elastic porous media*, preprint, 2019.
- [6] S. R. ARRIDGE, J. P. KAIPIO, V. KOLEHMAINEN, M. SCHWEIGER, E. SOMERSALO, T. TARVAINEN, AND M. VAUHKONEN, *Approximation errors and model reduction with an application in optical diffusion tomography*, Inverse Problems, 22 (2006), pp. 175–195.
- [7] A. BENSOUSSAN, J.-L. LIONS, AND G. PAPANICOLAOU, *Asymptotic Analysis for Periodic Structures*, North-Holland, Amsterdam, 1978.
- [8] V. I. BOGACHEV, *Measure Theory*, Springer-Verlag, Berlin, 2007.
- [9] D. CALVETTI, O. ERNST, AND E. SOMERSALO, *Dynamic updating of numerical model discrepancy using sequential sampling*, Inverse Problems, 30 (2014), 114019.
- [10] G. F. CAREY, S.-S. CHOW, AND M. K. SEAGER, *Approximate boundary-flux calculations*, Comput. Methods Appl. Mech. Engrg., 50 (1985), pp. 107–120.
- [11] D. CIORANESCU AND P. DONATO, *An Introduction to Homogenization*, Oxford Lect. Ser. Math. Appl. 17, Oxford University Press, New York, 1999.
- [12] M. DASHTI AND A. M. STUART, *The Bayesian approach to inverse problems*, in *Handbook of Uncertainty Quantification*, Springer, New York, 2016, pp. 1–118.
- [13] E. DE GIORGI AND S. SPAGNOLO, *Sulla convergenza degli integrali dell'energia per operatori ellittici del secondo ordine*, Boll. Un. Mat. Ital., 4 (1973), pp. 391–411.
- [14] M. M. DUNLOP AND A. M. STUART, *The Bayesian formulation of EIT: analysis and algorithms*, Inverse Probl. Imaging, 10 (2016), pp. 1007–1036.
- [15] M. M. DUNLOP, M. A. IGLESIAS, AND A. M. STUART, *Hierarchical Bayesian level set inversion*, Stat. Comput., 27 (2017), pp. 1555–1584.
- [16] C. FREDERICK AND B. ENGQUIST, *Numerical methods for multiscale inverse problems*, Commun. Math. Sci., 15 (2017), pp. 305–328.
- [17] M. A. GREPL, Y. MADAY, N. C. NGUYEN, AND A. T. PATERA, *Efficient reduced-basis treatment of nonaffine and nonlinear partial differential equations*, ESAIM Math. Model. Numer. Anal., 41 (2007), pp. 575–605.
- [18] M. A. IGLESIAS, Y. LU, AND A. STUART, *A Bayesian level set method for geometric inverse problems*, Interfaces Free Bound., 18 (2016), pp. 181–217.
- [19] N. LINDEA, D. GINSBOURGER, J. IRVING, F. NOBILE, AND A. DOUCETE, *On uncertainty quantification in hydrogeology and hydrogeophysics*, Adv. Water Resources, 110 (2017), pp. 166–181.
- [20] F. MURAT AND L. TARTAR, *H-convergence*, in *Topics in the Mathematical Modelling of Composite Materials*, Progr. Nonlinear Differential Equations Appl. 31, Birkhäuser Boston, Boston, MA, 1997, pp. 21–43.
- [21] F. NOBILE AND F. TESEI, *A multi level Monte Carlo method with control variate for elliptic PDEs with log-normal coefficients*, Stoch. Partial Differ. Equ. Anal. Comput., 3 (2015), pp. 398–444.
- [22] J. NOLEN AND G. PAPANICOLAOU, *Fine scale uncertainty in parameter estimation for elliptic equations*, Inverse Problems, 25 (2009), 115021.
- [23] J. NOLEN, G. A. PAVLIOTIS, AND A. M. STUART, *Multiscale modeling and inverse problems*, in *Numerical Analysis of Multiscale Problems*, Lect. Notes Comput. Sci. Eng. 83, Springer, New York, 2012, pp. 1–34.
- [24] A. M. STUART, *Inverse problems: A Bayesian perspective*, Acta Numer., 19 (2010), pp. 451–559.
- [25] A. TARANTOLA, *Inverse Problem Theory and Methods for Model Parameter Estimation*, SIAM, Philadelphia, PA, 2005.
- [26] J. XIE, Y. EFENDIEV, AND A. DATTA-GUPTA, *Uncertainty quantification in history matching of channeled reservoirs using Markov chain level set approaches*, Soc. Pet. Eng., 1 (2011), pp. 49–76.